CR-102724

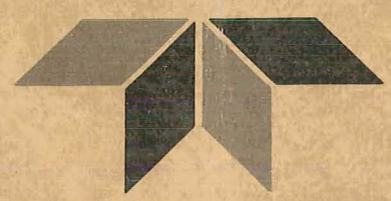TECHNICAL NOTE AST-275

Summary Report
Project TD-AAD-4-005

APPLICATION OF HEAT PIPES TO SPACECRAFT THERMAL CONTROL PROBLEMS

by J. L. Thurman
    S. Mei

July 1968

RESEARCH LABORATORIES

BROWN ENGINEERING

A TELEDYNE COMPANY

Research Park • Huntsville, Alabama 35807

TECHNICAL NOTE AST-275

APPLICATION OF HEAT PIPES TO SPACECRAFT
THERMAL CONTROL PROBLEMS

By

J. L. Thurman
S. Mei

July 1968

TECHNICAL NOTE AST-275

APPLICATION OF HEAT PIPES TO SPACECRAFT
THERMAL CONTROL PROBLEMS

By J. L. Thurman and S. Mei
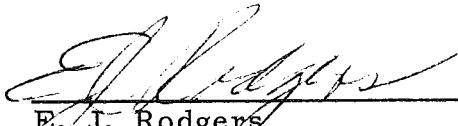Brown Engineering Company, Inc.

ABSTRACT

The applicability of heat pipes to the solution of thermal control
problems associated with future spacecraft, including the Saturn V work-
shop is investigated. The investigation includes a survey of reported
experience in heat pipe technology, an analysis of the effect of variation
in various design parameters on heat pipe performance, and establish-
ment of concepts utilizing the heat pipe which offer unique solutions to
specific thermal control problems. Concepts are described and analyzed
which appear applicable to the solution of problems of cryogenic boiloff
control, temperature nonuniformity of skin structure, removal of heat
from concentrated sources and radiator design.

Approved:

H. C. Crews, Jr.
Manager
Space and Military Systems Division

Approved: Approved:

E. J. Rodgers   R. C. Watson, Jr.
Associate Director of Research   Vice President
                                       Advanced Systems and Technologies

iii

TABLE OF CONTENTS

TABLES OF CONTENTS - Concluded

LIST OF ILLUSTRATIONS

LIST OF ILLUSTRATIONS - Concluded

LIST OF SYMBOLS

Symbol	Definition
A_b	Area of boiling heat transfer surface, ft^2
A_c	Cross-sectional area of heat pipe wall, ft^2
A_s	Fiber surface area per unit volume of wick, ft^2/ft^3
A_w	Area of wick, ft^2
B	Spacing between heat pipes, ft
b	Dimensionless constant depending on the detailed geometry of the capillary structure; for nonconnected parallel cylindrical pores $b \approx 8$; for realistic capillary structure with interconnected pores $b \approx 10$ to 20.
c_p	Specific heat, Btu/lbm-°R
$c_{p\ell}$	Specific heat of liquid in wick, Btu/lbm-°R
De	Dimension parameter used in calculating wick boiling heat transfer coefficient, ft
D_f	Mean fiber diameter, ft
D_i	Inside diameter of tube, ft
G'	Mass flux of liquid through wick $(Q_e/A_b \epsilon \lambda)$, lbm/hr-$ft^2$
g	Local acceleration of gravity, ft/sec^2
g_c	Dimensional constant, 32.2 lbm-ft/lbf-sec^2
h	Average heat transfer coefficient, Btu/hr-ft^2-°R
h_b	Wick boiling heat transfer coefficient, Btu/hr-ft^2-°R
h_c	Average condensation heat transfer coefficient, Btu/hr-ft^2-°R

LIST OF SYMBOLS - Continued

Symbol	Definition
k	Correction term for channel shape
k_ℓ	Thermal conductivity of condensate film, Btu/hr-ft-°R
k_p	Thermal conductivity of heat pipe wall, Btu/hr-ft-°R
k_s	Thermal conductivity of spacecraft skin material, Btu/hr-ft-°R
L	Length of heat pipe, ft
L_e	Length of evaporator section, ft
M	Molecular weight of working fluid, lbm/mole
$\dot{m}_\ell(z)$	Axial liquid flow rate in wick at position z, lbm/hr
$\dot{m}_v(z)$	Axial flow of vapor at position z, lbm/hr
N	Number of channels cut into inside surface of tube
n	Unit normal vector to cylindrical surface
P	Perimeter of container at inside surface, ft
Pr	Prandtl number
Pr_ℓ	Prandtl number of liquid in wick
p	Absolute pressure of liquid, lbf/ft^2
p_ℓ	Local pressure of liquid in heat pipe capillary structure, lbf/ft^2
p'_ℓ	Vapor pressure of liquid, lbf/ft^2
p_v	Local pressure of vapor in heat pipe core, lbf/ft^2
$p'_{\ell L}$	Vapor pressure of liquid at condenser end, lbf/ft^2

LIST OF SYMBOLS - Continued

Symbol	Definition
p'_{l_O}	Vapor pressure of liquid at evaporator end, lbf/ft^2
p_{v_L}	Local pressure of vapor at condenser end of heat pipe, lbf/ft^2
p_{v_O}	Local pressure of vapor at evaporator end of heat pipe, lbf/ft^2
Q_e	Total rate of heat added in evaporator section of heat pipe, Btu/hr
Q_c	Total rate of heat removal from condenser section of heat pipe, Btu/hr
Q_{max}	Maximum power limit of heat pipe, Btu/hr
Q_s	Local total absorbed irradiation flux, including solar, albedo, planetshine, $Btu/hr\text{-}ft^2$
q_{max}	Maximum limiting radiation flux, $Btu/hr\text{-}ft^2$
$\overline{R}$	Universal gas constant, 1.986 Btu/mole-°R
Re	Reynolds number
R_r	Reynolds number of vapor in heat pipe, $\rho_v V_r r_v / \mu_v$
r	Radius of curvature of vapor-liquid interface in capillary structure or effective channel radius, ft
$\overline{r}$	Mean radius of outer skin, ft
r_b	Critical bubble radius of curvature above which boiling will occur in the wick, ft
r_c	Minimum pore radius of capillary structure, ft
r_h	Hydraulic radius, ft
r_o	Radius of outer skin structure, ft

Symbol	Definition
r_v	Radius of vapor passage, ft
r_w	Inside radius of containing envelope, ft
T	Temperature of heat pipe wall; temperature of metal skin between heat pipes, °R
T_i	Temperature of liquid-vapor interface, °R
T_o	Average effective vapor temperature at heat pipe, °R
ΔT_{sat}	Difference between saturated vapor and condensing surface temperature, °R
T_v	Vapor temperature inside heat pipe, °R
T_w	Wall temperature of heat pipe, °R
v_r	Radial velocity of vapor at inside wall of vapor chamber, ft/hr
x	Axial distance from station midway between heat pipes, ft
z	Axial distance from evaporator end of heat pipe, ft
α	Numerical factor (≈ 1) including the probability of condensation of an impinging vapor molecule and the roughness of the meniscus interface formed on the capillary structure
δ	Spacecraft skin thickness, ft
ϵ	Fraction of wick volume occupied by liquid (porosity); emissivity of outer skin surface
η	Symbol defined on page 9
θ	Contact angle between liquid and capillary structure, radians; circumferential angle shown by Figure , radians
λ	Latent heat of vaporization of liquid, Btu/lbm
μ_ℓ	Dynamic viscosity of liquid in wick, lbm/hr-ft

LIST OF SYMBOLS - Concluded

Symbol	Definition
μ_v	Dynamic viscosity of vapor, lbm/hr-ft
ν_ℓ	Kinematic viscosity of liquid in wick, ft^2/sec
ν_v	Kinematic viscosity of vapor, ft^2/sec
ρ_f	Fiber density, lbm/ft^3
ρ_ℓ	Density of liquid in wick, lbm/ft^3
ρ_v	Local vapor density, lbm/ft^3
ρ_{wi}	Density of fiber-void mesh, lbm/ft^3
σ	Surface tension of working fluid in contact with capillary structure, lbf/ft; also, Stefan-Boltzman constant, $0.1718 \, (10^{-8})$ Btu/hr-ft^2-$°R^4$
ϕ	Angle of heat pipe inclination from horizontal, deg

TECHNICAL NOTE AST-275

APPLICATION OF HEAT PIPES TO SPACECRAFT
THERMAL CONTROL PROBLEMS

SUMMARY

An investigation of the applicability of heat pipes to the solution of complex thermal control problems associated with future spacecraft was conducted, with emphasis on the Saturn V workshop.

A complete literature survey of heat pipe technology was performed, dating back to the introduction of the heat pipe concept in 1964. The literature survey is summarized in Appendix A.

A parametric analysis to determine the effects of variation in geometrical design parameters on the maximum power limit of heat pipes, considering water as the working fluid, is presented. Uniform heat addition and removal along the heat pipe is assumed. Calculations were performed resulting in parametric curves which show the variation in maximum power limit with variables such as heat pipe length, inside pipe diameter, vapor passage radius, and wick porosity and pore size. Candidate working fluids for different ranges of operating temperature are compared by curves of calculated maximum power limit of each fluid as a function of operating temperature, considering fixed heat pipe geometry. A brief discussion of wick characterization is also included.

Concepts, utilizing the heat pipe, were established which offer unique solutions to certain thermal control problems, as described below:

* A boiloff reduction system for stored cryogens is discussed, which appears promising for cryogens having relatively high boiling temperatures, such as liquid oxygen. The system appears impractical for liquid hydrogen, except for very small stored quantities.

- The use of heat pipes to improve the temperature uniformity of nonuniformly irradiated skin structures is analyzed mathematically and a procedure established for performing computations.

- A thermal analysis is performed of the application of heat pipes to the removal of heat from a concentrated source. This concept is applicable to the cooling of electronic components and other such heat sources. An equation is derived for calculating the axial wall temperature distribution near the ends of a heat pipe which receives and rejects heat by axial conduction through the annular pipe wall. It is shown that the axial temperature gradient dissipates very near the ends and that most of the heat pipe length is essentially isothermal. Even the temperature gradients near the ends can be eliminated by radial addition and removal of heat over a large surface area, as has been demonstrated by numerous experiments cited in the literature.

- Another application of heat pipes which is attractive in some situations lies in the improvement of space radiator efficiency. By employing the heat pipe concept, the radiator can be made to operate at a higher average temperature, resulting in less required surface area than for conventional radiators. Although a weight savings may not be realized over radiators that are integrated into the vehicle skin structure and use the skin as the radiating fin, the concept may be advantageous in situations which demand a deployable radiator.

The heat pipe applications suggested in this investigation represent only a few of the many applications which can be expected to be discovered after subsystems are defined more clearly and designs progress further.

2

SECTION I. INTRODUCTION

This study was conducted under Contract NAS8-20073 for the NASA George C. Marshall Space Flight Center to investigate the applicability of heat pipes to the solution of thermal control problems associated with future spacecraft, including the Saturn V workshop. The heat pipe (Ref. 1) is a self-contained, engineering structure which utilizes the phase change and surface tension characteristics of a working fluid to transport large quantities of heat between source and sink with very small temperature drop.

In recent years considerable work has been devoted to developing the heat pipe for application to nuclear space power supplies. In the nuclear power application heat pipes are used to transfer heat isothermally from the reactor core to a thermionic converter some distance away and to improve the efficiency of and reduce the weight of the waste heat radiator.

Such an effective heat transfer device should find many applications in solving complicated thermal control problems of future spacecraft, e. g., transferring heat efficiently from a concentrated heat source, such as an electronic component, to a heat exchanger or radiator. A few obvious applications have been analyzed in the present study. As subsystems are more clearly defined, many more useful applications may be expected to be discovered.

Also included in this study is a parametric analysis illustrating the relative importance of pertinent geometrical and working fluid parameters on the maximum heat transfer rates that may be accommondated by heat pipes.

4

SECTION II.   HEAT PIPE OPERATION

A.   Basic Principles

As illustrated by Figure 1, the heat pipe consists of a sealed container whose inside walls are lined with a capillary structure (wick) which is saturated with a liquid (working fluid) at a certain operating pressure. As heat is added to one end of the pipe, termed the evaporator, the liquid in the adjacent wick evaporates, absorbing its latent heat. The generated vapor flows from the hot end to the cooler, condenser end because of the resulting difference in vapor pressure, where the vapor condenses onto the wick and gives up its latent heat.
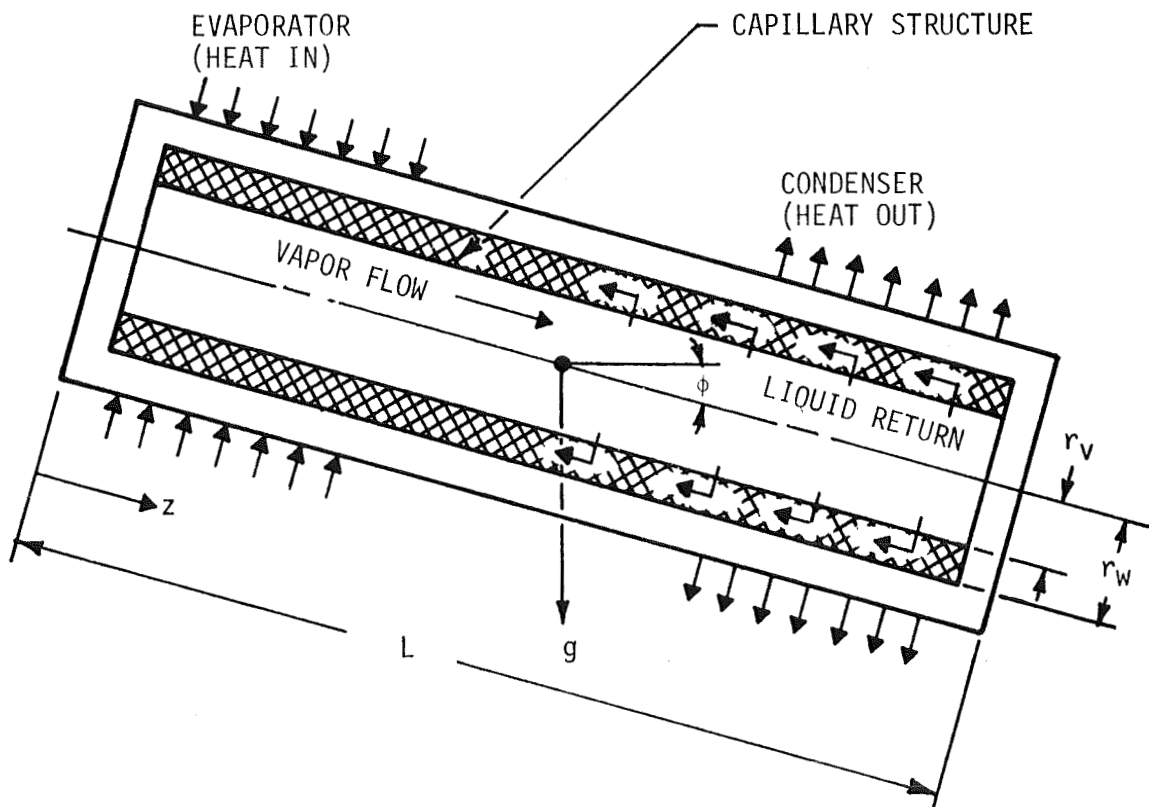
FIGURE 1.   SCHEMATIC OF A HEAT PIPE

The evaporation of liquid at the vapor-liquid interface causes the residual liquid to retreat into the capillary structure, giving a meniscus radius of curvature and contact angle which are smaller in the evaporator than in the condenser section, where the condensate is being deposited. This causes a pressure difference in the liquid which pumps it through the wick from the condenser section back to the evaporator section, thus completing the cycle.

Although the heat pipe is an extremely effective heat transfer device, it must operate within certain design limitations. The maximum total power that can be transferred in a heat pipe of given size and with a given fluid is determined by the ultimate pumping capacity of the capillary structure and by the onset of film boiling between the pipe wall and the wick. It has been noted in the literature that in past experiments, the capillary pumping limitation is more prevalent than the film boiling limitation if metal wick structures are used.

The pumping capacity of the capillary structure depends on the size and geometry of the wick, as well as on the properties of the working fluid, such as its latent heat of vaporization, surface tension, density, and viscosity. The functional relationship between the ultimate pumping capacity of the wick and its geometrical factors, as well as the properties of the working fluid, can be obtained by applying general conservation equations to the system.

As mentioned previously, the primary limiting condition for heat pipe operation is determined by the maximum capillary pumping force, which must be equal to or greater than all the losses in a complete cycle. The necessary relationship for continuous fluid circulation is described by the following equation

$$
\boxed{\begin{array}{c}\text{Pressure}\\\text{Drop in}\\\text{the Vapor}\end{array}} + \boxed{\begin{array}{c}\text{Pressure Head}\\\text{in the Liquid}\\\text{Due to Gravity}\end{array}} + \boxed{\begin{array}{c}\text{Frictional}\\\text{Pressure Drop}\\\text{in the Liquid}\end{array}} \leq \boxed{\begin{array}{c}\text{Pressure Rise}\\\text{Due to Capillary}\\\text{Forces}\end{array}} \qquad (1)
$$

Applying the general principles of conservation of mass, momentum, and energy to the system under steady-state condition, Cotter (Ref. 2) was able to obtain expressions for the pressure drop in the vapor and liquid, and the pressure head loss due to gravity. Only the results of Cotter's analysis are presented here. A more detailed discussion of the derivation is included in Appendix A.

The vapor pressure drop in the direction of vapor flow for uniform axial heat addition to the removal from a heat pipe was found to be

$$
\text{Pressure Drop in Vapor} =
\begin{cases}
+ \dfrac{4\,\mu_v\,L\,Q_e}{\pi\,\rho_v\,r_v^{\,4}\,\lambda\,g_c} & R_r \ll 1 \\[4mm]
+ \dfrac{(1 - 4/\pi^2)\,Q_e^{\,2}}{8\,\rho_v\,r_v^{\,4}\,\lambda^2\,g_c} & R_r \gg 1
\end{cases}
\tag{2}
$$

The frictional pressure drop in the liquid and the heat loss due to gravity were given by

$$
\text{Frictional Pressure Drop in Liquid} = \frac{b\,\mu_\ell\,Q_c\,L}{2\,\pi\,(r_w^{\,2} - r_v^{\,2})\,\rho_\ell\,\epsilon\,r_c^{\,2}\,\lambda\,g_c}
\tag{3}
$$

$$
\text{Pressure Head in Liquid Due to Gravity} = \frac{g}{g_c}\,\rho_\ell\,\sin\phi\,L
\tag{4}
$$

Substituting Equations 2, 3, and 4 together with the pressure rise due to capillary forces,

$$
\text{Pressure Rise Due to Capillary Forces} = \frac{2\,\sigma\,\cos\theta}{r_c}
\tag{5}
$$

into Equation 1, one obtains Cotter's equation for maximum heat transfer rate at $R_r \gg 1$.

$$
\frac{2\,\sigma\,\cos\theta}{r_c} \geq \frac{(1 - 4/\pi^2)}{8\,\rho_v\,r_v^{\,4}\,\lambda^2\,g_c}\,Q_{max}^{\,2} + \frac{g}{g_c}\,\rho_\ell\,L\,\sin\phi
$$

$$
+ \frac{b\,\mu_\ell\,Q_{max}\,L}{2\,\pi\,(r_w^{\,2} - r_v^{\,2})\,\rho_\ell\,\epsilon\,r_c^{\,2}\,\lambda\,g_c}\,.
\tag{6}
$$

Letting

$$A = \frac{(1 - 4/\pi^2)}{8 \, \rho_v \, r_v^4 \, \lambda^2 \, g_c} \quad ;$$

$$B = \frac{b \, \mu_\ell \, L}{2\pi \, (r_w^2 - r_v^2) \, \rho_\ell \, \epsilon \, \lambda \, g_c} \quad ;$$

$$C = 2 \, \sigma \, \cos \theta \quad ;$$

$$D = \frac{g}{g_c} \, \rho_\ell \, L \, \sin \phi \quad ; \tag{7}$$

Equation 6 can be written as

$$A \, Q_{max}^2 + \frac{B}{r_c^2} \, Q_{max} - \frac{C}{r_c} + D = 0. \tag{8}$$

Solving Equation 8 for Q_{max}, one obtains the maximum power limit for heat pipes considering uniform heat addition and removal,

$$Q_{max} = \frac{-B + [B^2 - 4 \, A \, r_c^2 \, (D \, r_c^2 - C \, r_c)]^{\frac{1}{2}}}{2 \, A \, r_c^2} . \tag{9}$$

Substituting Equation 7 into Equation 9 and rearranging one obtains

$$Q_{max} = 0.341 \, A_v \, (L/r_c^2) \, \mu_v \, \lambda \, \{- \, (\nu_\ell / \nu_v) \, (A_v/A_{w,v}) \, (b/\epsilon)$$

$$+ [(\nu_\ell / \nu_v)^2 \, (A_v/A_{w,v})^2 \, (b/\epsilon)^2$$

$$- \, 23.48 \, \eta \, (r_c/L)^2 \, (N_v \, r_c/\mu_v \, \lambda) \, \cos \theta]^{\frac{1}{2}} \} \tag{10}$$

where

$$A_v = \pi \, r_v^2$$

$$A_{w,v} = \pi \, (r_w^2 - r_v^2)$$

$$\frac{\nu_\ell}{\nu_v} = \frac{\mu_\ell \, \rho_v}{\mu_v \, \rho_\ell}$$

$$\eta = \frac{g}{g_c} \frac{\rho_\ell \, L \, r_c \sin \phi}{2 \, \sigma \cos \theta} - 1$$

$$N_v = \frac{\sigma \, \rho_v \, \lambda}{\mu_v} \quad .$$

Equation 10 was programmed for digital computer solution to permit rapid evaluation of the effect of variation in geometrical factors and working fluid properties on maximum power limit of heat pipes. The results of this analysis are discussed in Section II-B.

As stated above, another limitation on the maximum power limit of heat pipes is the onset of film boiling between the pipe wall and the wick. Since the temperature at the liquid-vapor interface is always the saturation temperature, the liquid in the capillary structure at the evaporator section is thus superheated, and the maximum superheat is possessed by the liquid closest to the pipe wall. If the amount of superheat at this point is large enough so that nucleation occurs, then a vapor blanket will be formed which can sharply reduce the heat transfer from the input surface. The result of film boiling can be burnout of the pipe wall. The boiling heat transfer encountered in the heat pipe is much more difficult than in ordinary pool boiling of liquid, because of the complexity of interaction of boiling with the overall circulation of liquid throughout the capillary structure. Generally, there is no useful experimental information available for the heat pipe boiling problem. However, a conservative criterion for nonoccurrence of boiling can be developed. A bubble will be formed at a nucleation cavity when the vapor pressure within the cavity is greater than the pressure in the surrounding liquid by an amount

$$p_v - p_\ell = \frac{2 \, \sigma}{r_b} \tag{11}$$

where r_b is the bubble radius. If the pressure difference is less than $2 \sigma / r_b$, then the bubble will collapse. Furthermore, in the capillary structure r_b cannot exceed r (= $r_c \sin \theta$). This implies that

$$\frac{1}{r_b} > \frac{1}{r_c \, \sec \theta} = \frac{\cos \theta}{r_c} \quad . \tag{12}$$

Thus, as long as the following holds,

$$p_v - p_\ell \leq \frac{2 \, \sigma \, \cos \, \theta}{r_c} \quad , \tag{13}$$

bubbles cannot grow beyond the critical size, and true boiling will not occur. Eastman (Ref. 3) indicated that the high purity of the fluid and the motion of the fluid through the capillary structure and across the heat-input surface tend to prevent the formation of bubbles. However, there is still a maximum input power density that cannot be exceeded. Input power densities, exceeding this critical value, will cause the burn-out of the heat pipe. For example, the critical heat flux density for water at 212° F is 3.2 × 10^5 Btu/hr-ft^2 of evaporator surface, or 1.6 × 10^6 Btu/hr-ft^2 for lithium at 2 700° F.

B. Effect of Variation in Design Parameters on Maximum Heat Transfer Rate

Equation 10 was utilized to analyze the effects of variation in geometrical design parameters on maximum heat transfer rate, considering water at 150° F as the working fluid. Prior to the parametric analysis certain baseline values of the design variables were established around which the perturbation was performed. The selected values are listed in Table 1.

TABLE 1. BASELINE VALUES FOR PARAMETRIC ANALYSIS OF HEAT PIPES

	Value
Heat pipe length (L), ft	3
Inside pipe diameter (2 r_w), in.	2
Vapor passage diameter (2 r_v), in.	1.33
Mean pore radius of wick (r_c), ft	0.00125
Wick geometrical factor (b)	12
Wick porosity (ε)	0.8
Acceleration of gravity (g), ft/sec^2	0

The results of the analysis are shown in Figures 2 through 10. The dependence of maximum power limit on r_v/r_w (the ratio of vapor passage radius to inside pipe radius) with length as a parameter is shown in Figures 2 through 4. For lengths of 3 and 5 feet, the maximum power limit passes through a maximum at an optimum ratio of r_v/r_w of 0.67. This result was predicted analytically by Cotter (Ref. 2). For a length of 1 foot, an optimum value of r_v/r_w was not indicated, although it could have fallen between the points tested. As the pipe inside diameter is increased from 1 to 2, and then to 3 inches, the maximum power limit increases from 5 500 to 49 000 Btu/hr for the baseline length of 3 feet, as shown by comparison of Figures 2, 3, and 4.

Figure 5 shows the variation of maximum power limit with heat pipe length at various values of mean pore radius of the wick. In all cases the maximum power limit decreases with increasing length, due to the longer path of condensate return. It is noted that increasing the pore radius reduces the sensitivity of maximum power limit to length, because the frictional pressure drop of the liquid in the wick is smaller.

The variation of maximum power limit with heat pipe inside radius is shown in Figure 6 for various values of r_v/r_w. Increasing the pipe inside radius results in a larger maximum power limit. Of the r_v/r_w ratios tested, a value of 0.67 yielded the largest heat transfer limit, as predicted by Cotter (Ref. 2).

Figures 7 through 9 show the variation of maximum power limit with r_v/r_w at various values of mean pore radius of the wick. Of the values tested, a mean pore radius of 0.00125 foot yielded the largest maximum power limit; and the optimum ratio of r_v/r_w was again 0.67 except for the mean pore radius of 0.0025 foot. No optimum was indicated for this value, although it again could have fallen between the points tested. Comparison of Figures 7, 8, and 9 shows that an pipe inside diameter is increased, the maximum power limit increases, as expected.

Figure 10 shows the variation in maximum power limit with wick porosity, ϵ, at different values of the dimensionless geometrical factor b. Although b is poorly defined in the literature, Cotter (Ref. 2) suggested that its value is approximately 8 for parallel non-connected cylindrical pores, and lies between 10 to 20 for realistic
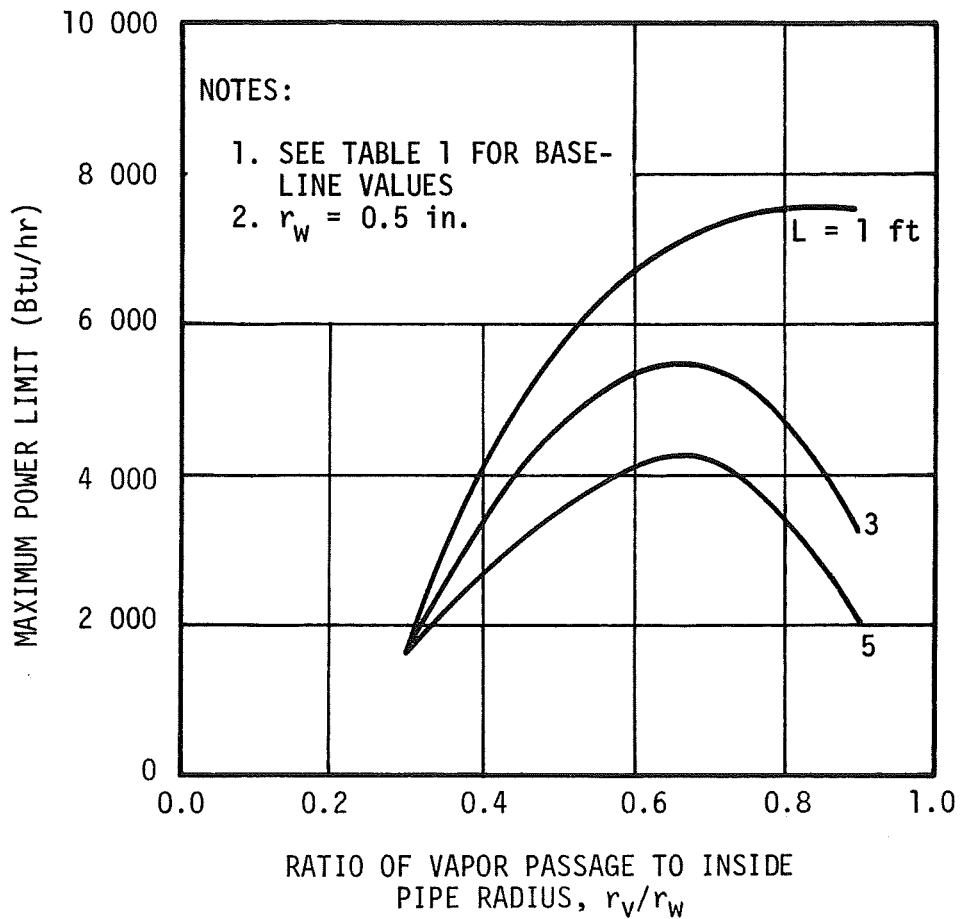
FIGURE 2. MAXIMUM POWER LIMIT AS A FUNCTION OF RATIO OF VAPOR PASSAGE
RADIUS TO INSIDE PIPE RADIUS CONSIDERING VARIOUS HEAT PIPE
LENGTHS (PIPE INSIDE DIAMETER = 1 in.)
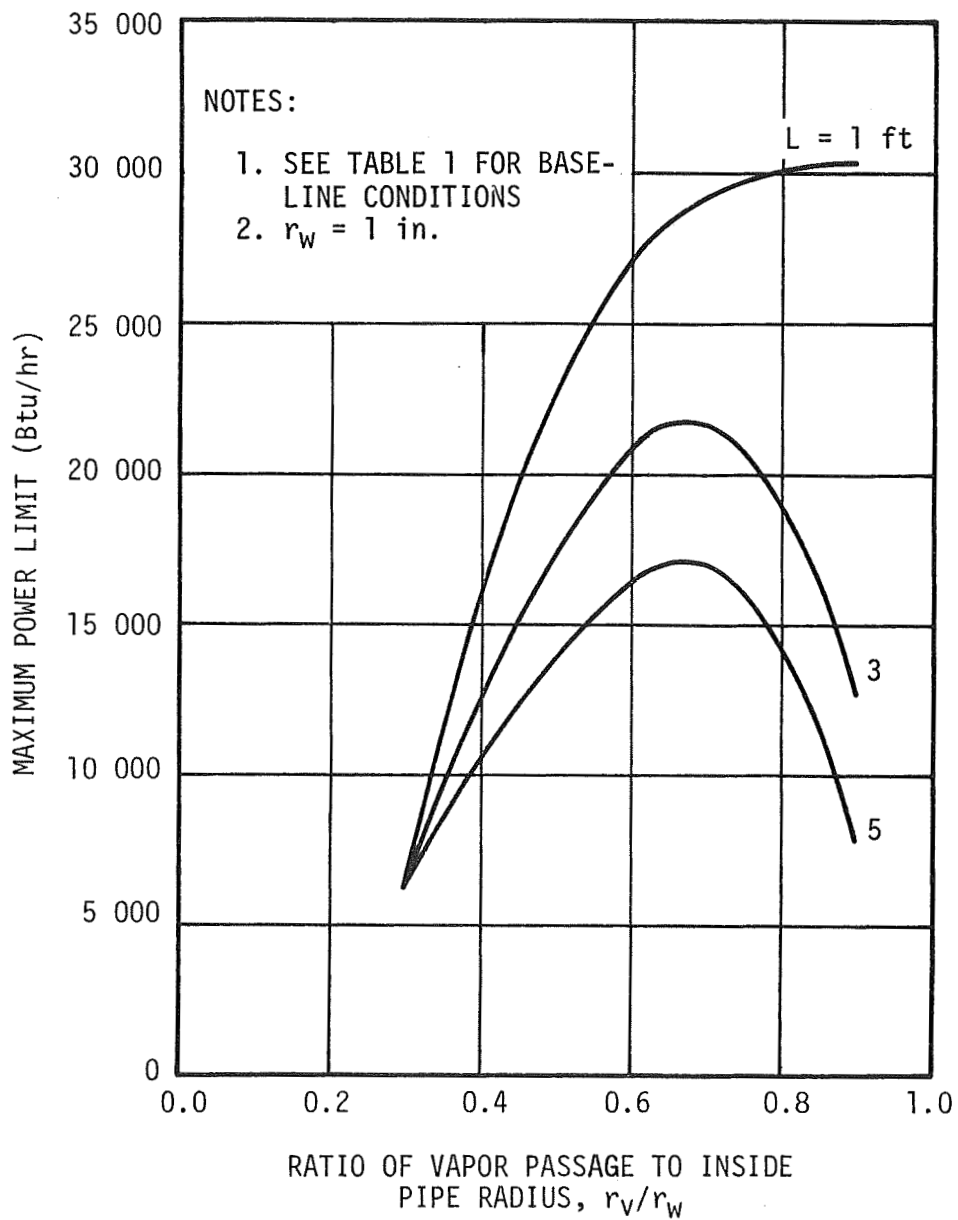
FIGURE 3. MAXIMUM POWER LIMIT AS A FUNCTION OF RATIO OF VAPOR PASSAGE
RADIUS TO INSIDE PIPE RADIUS CONSIDERING VARIOUS HEAT PIPE
LENGTHS (PIPE INSIDE DIAMETER = 2 in.)
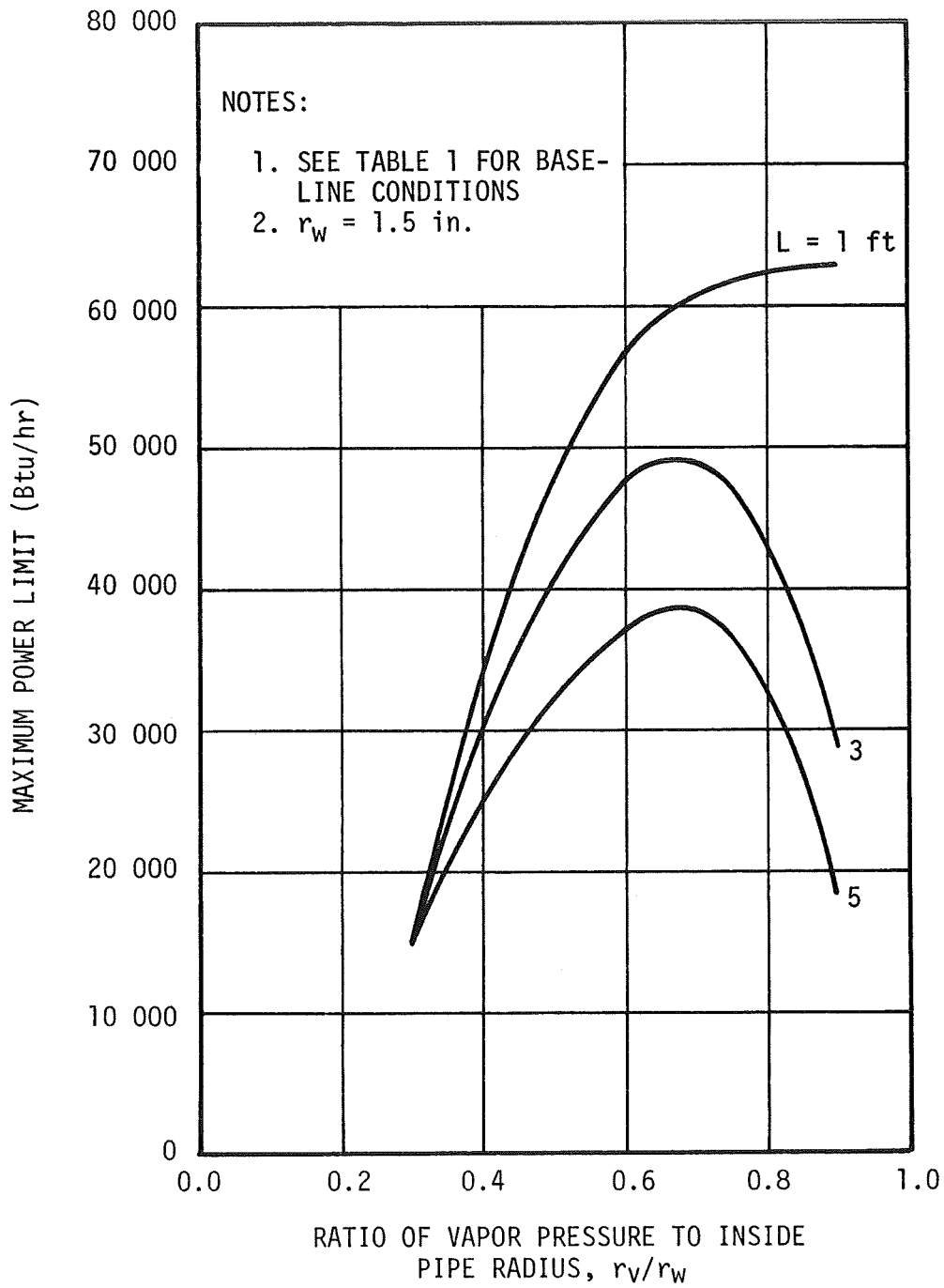
FIGURE 4. MAXIMUM POWER LIMIT AS A FUNCTION OF RATIO OF VAPOR PASSAGE RADIUS TO INSIDE PIPE RADIUS CONSIDERING VARIOUS HEAT PIPE LENGTHS (PIPE INSIDE DIAMETER = 3 in.)
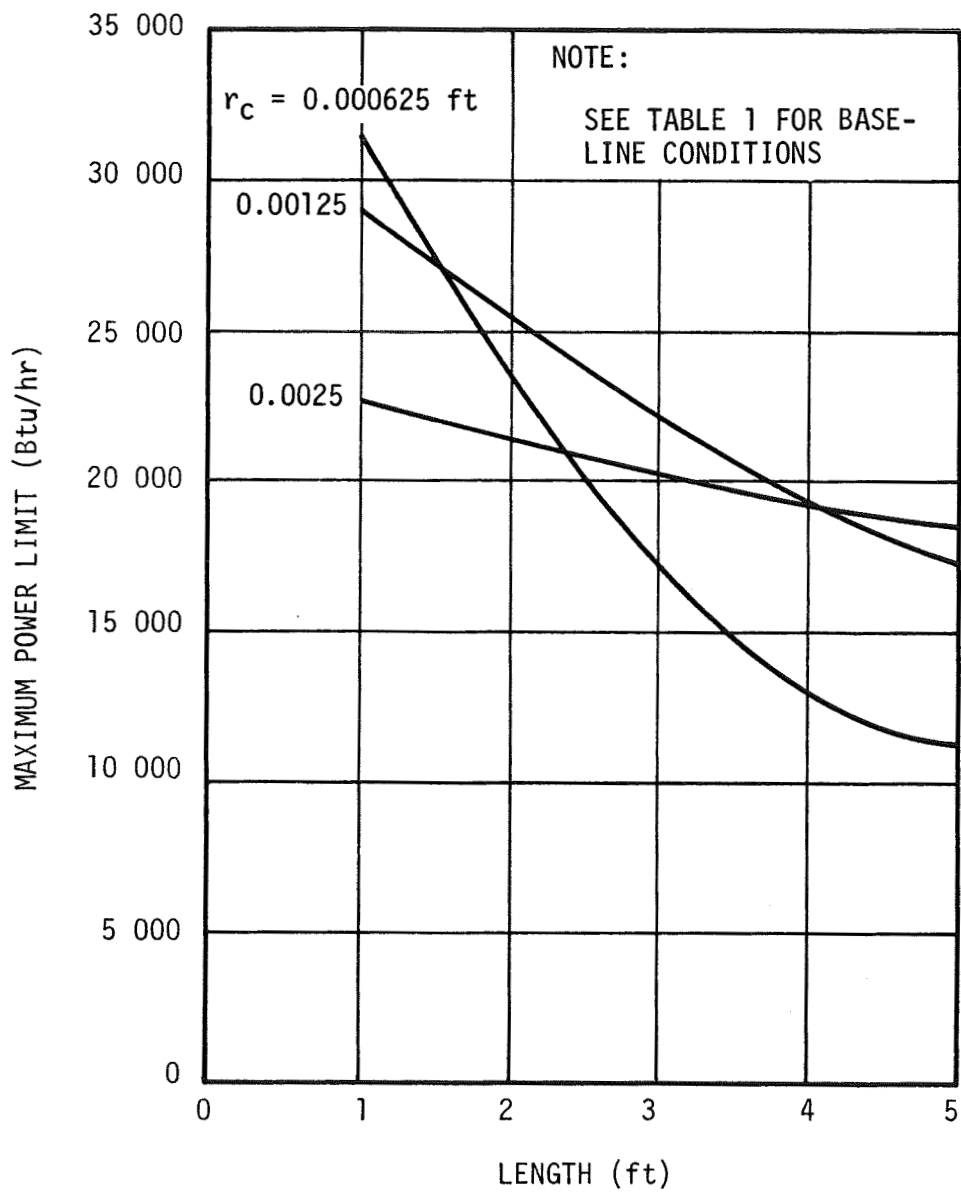
FIGURE 5. MAXIMUM POWER LIMIT AS A FUNCTION OF HEAT PIPE LENGTH
AT VARIOUS VALUES OF MEAN PORE RADIUS

NOTE:

SEE TABLE 1 FOR BASELINE
CONDITIONS

$r_V/r_W = 0.67$

0.9

0.3

MAXIMUM POWER LIMIT (Btu/hr)

70 000

60 000

50 000

40 000

30 000

20 000

10 000

0

0.000   0.020   0.040   0.060   0.080   0.100   0.120

INSIDE PIPE RADIUS, r_W (ft)
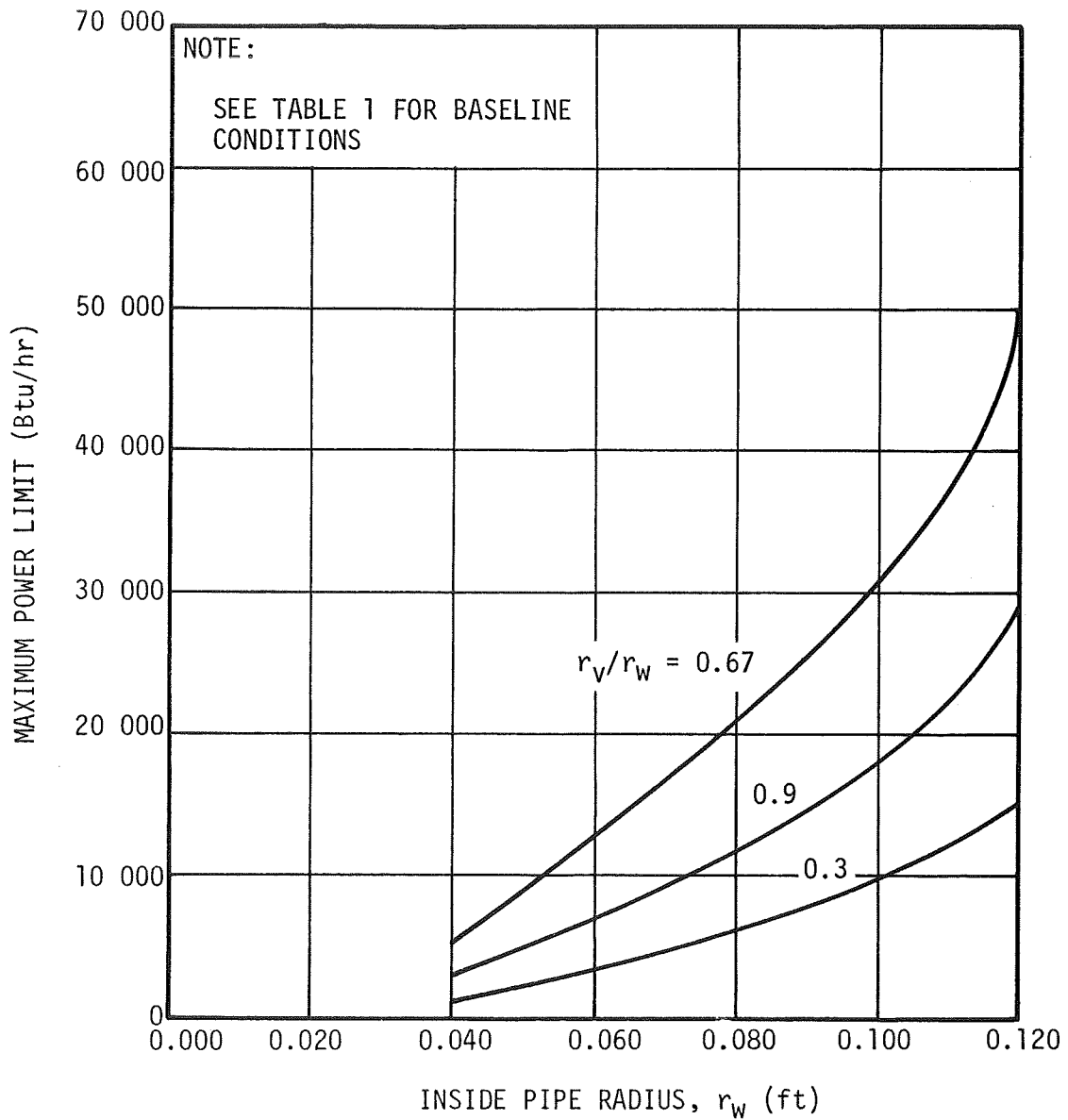
FIGURE 6.   MAXIMUM POWER LIMIT AS A FUNCTION OF INSIDE HEAT PIPE RADIUS
AT VARIOUS r_V/r_W RATIOS

16
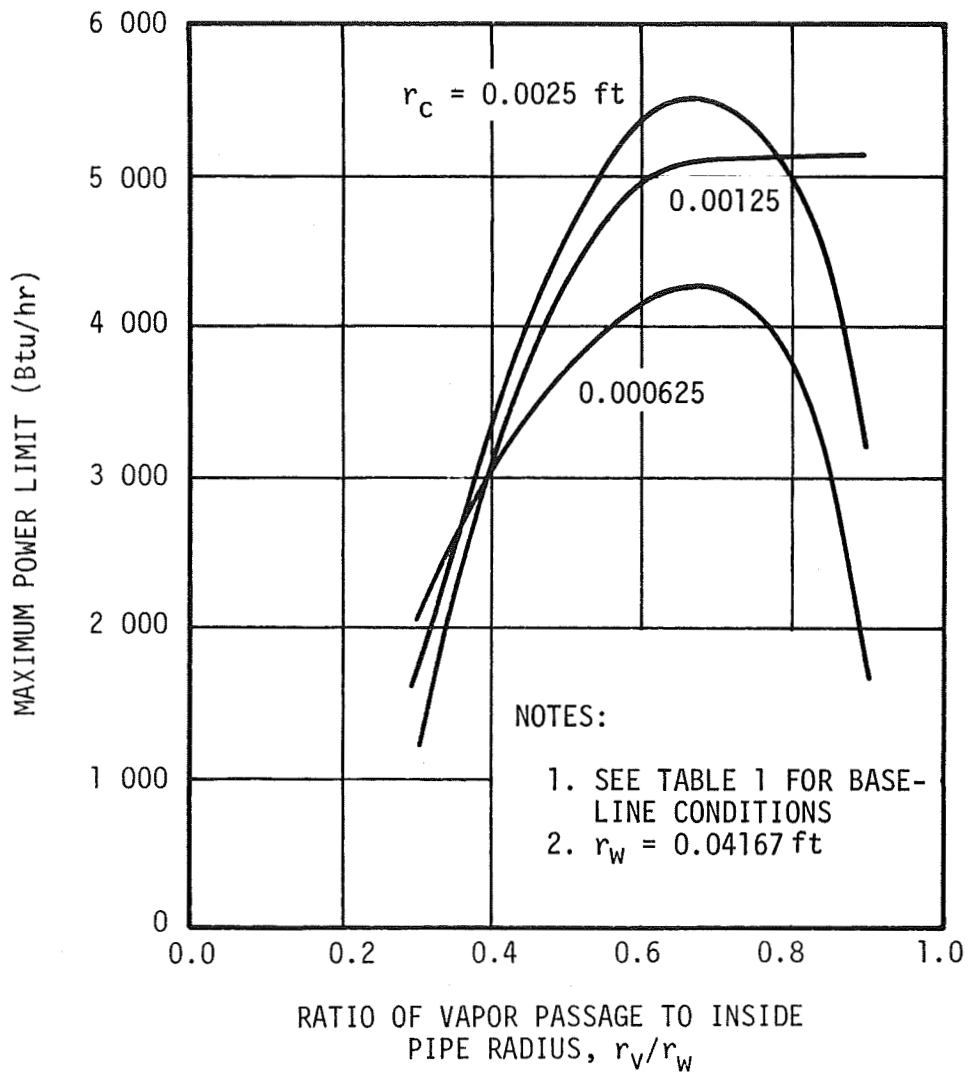
FIGURE 7. MAXIMUM POWER LIMIT AS A FUNCTION OF r_V/r_W AT VARIOUS VALUES OF WICK MEAN PORE RADIUS (PIPE INSIDE DIAMETER = 1 in.)
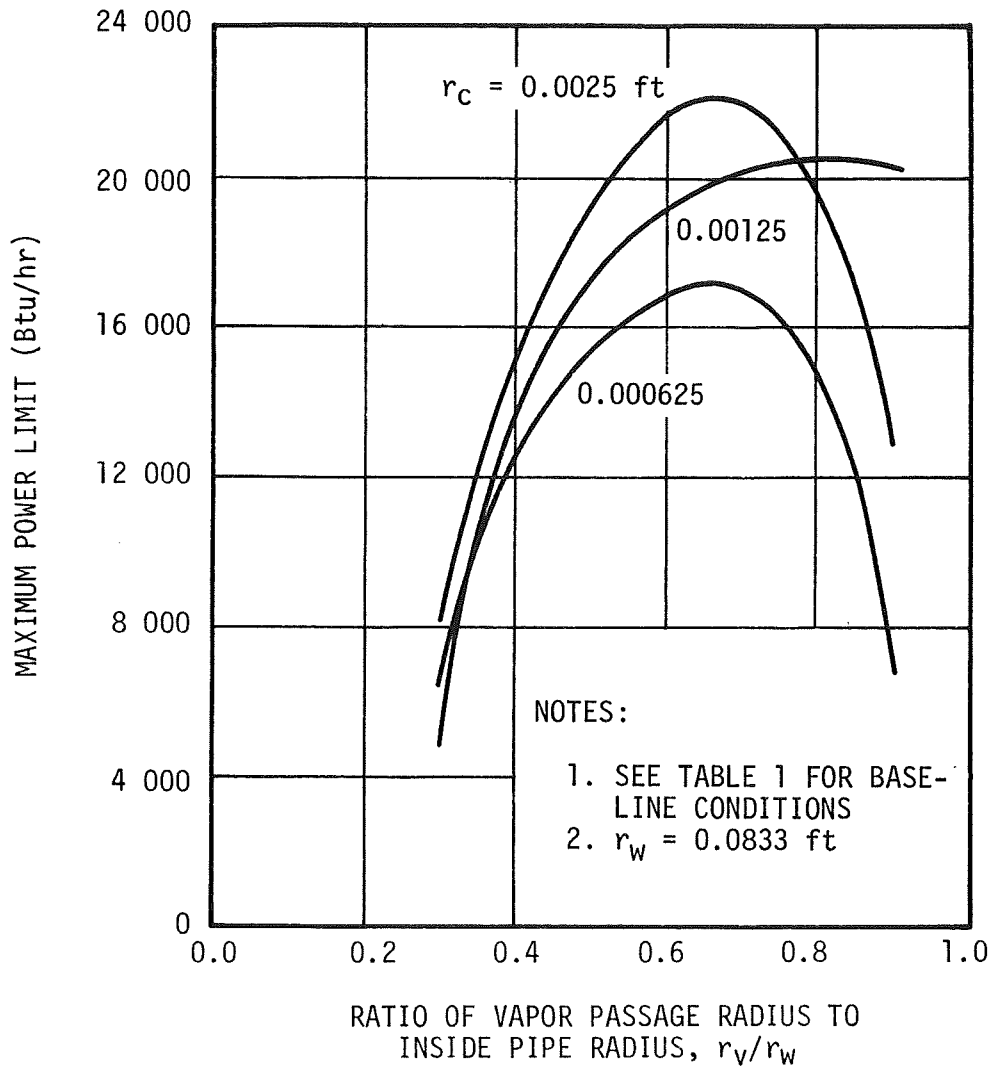
FIGURE 8. MAXIMUM POWER LIMIT AS A FUNCTION OF r_V/r_W AT VARIOUS VALUES OF WICK MEAN PORE RADIUS (PIPE INSIDE DIAMETER = 2 in.)

18
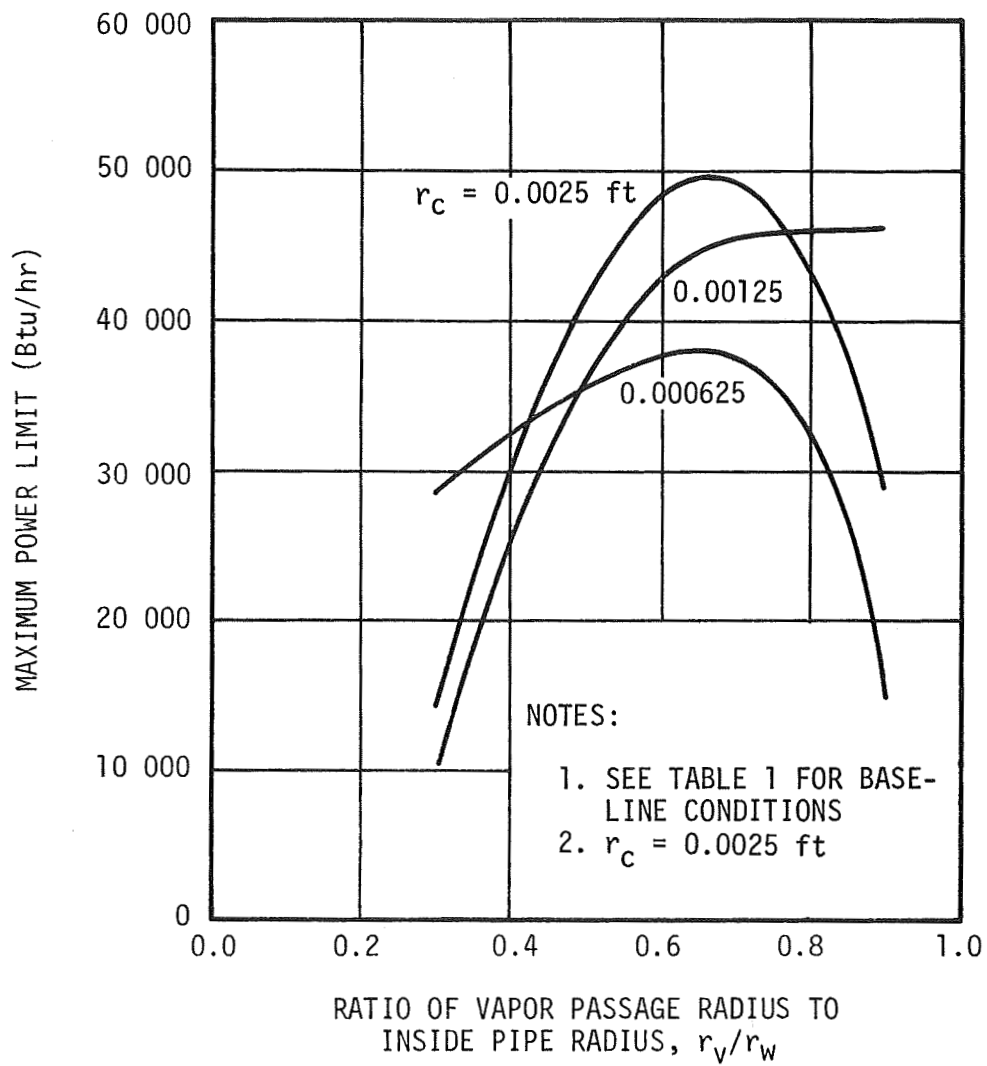
FIGURE 9. MAXIMUM POWER LIMIT AS A FUNCTION OF r_v/r_w AT VARIOUS
VALUES OF WICK MEAN PORE RADIUS
(PIPE INSIDE DIAMETER = 3 in.)

19
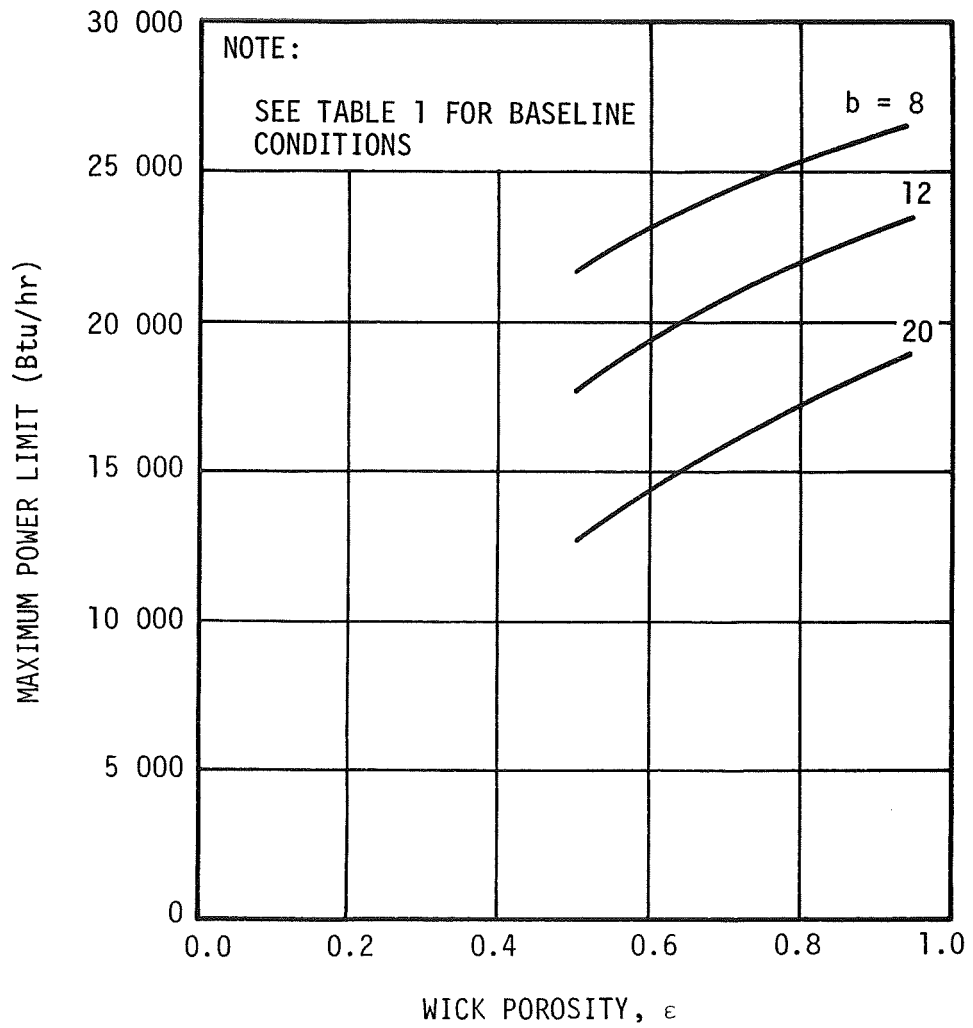
FIGURE 10. MAXIMUM POWER LIMIT AS A FUNCTION OF POROSITY FOR VARIOUS VALUES OF b

capillary structures with interconnected pores. Kemme (Ref. 4) reported a value of b = 12 for a certain wick structure. Since b is so poorly understood, values of 8, 12, and 20 were tested to determine its effect on maximum heat transfer rate. As shown by Figure 10, smaller values of b yield larger heat transfer limits.

It was intended to test the effects of gravity and inclination angle on the heat transfer limit, but a negative radical was encountered in Equation 10 due to η being positive. This was caused by the unintentional selection of test values of mean pore radii, r_c, which were too large, thus yielding positive values of η and a negative radical. Lack of time prevented reselection of test variables. However, this obstacle pointed out the importance of selecting r_c in future gravity designs such that the term η is negative, thus yielding a positive radical.

C. Comparison of Working Fluids

Selection of a good working fluid is vital to proper heat pipe design. The choice of fluids starts tentatively with a boiling point that coincides with the desired operating temperature. Moreover, at this operating temperature the fluid saturation pressure must be small enough that containment is not a serious problem, and a thin-walled pipe can be used for good heat transfer and light weight. The compatibility of the working fluid with enclosure and wick materials is also a consideration, although the usual procedure will be to select wick and enclosure materials to be compatible with a chosen working fluid since more flexibility exists with structural materials than with working fluids.

In the selection of working fluids, certain desirable properties may be listed immediately from physical reasoning. These are

- Suitable boiling point

- High latent heat

- High surface tension

- High thermal conductivity

- Good wetting ability

- Noncorrosive

- Nontoxic

- Inert to chemical decomposition.

It is also important to select a working fluid such that the heat pipe will have a large maximum power limit. Examination of Equation 10 provides a criterion for selecting fluids which will yield the large power limit. Considering a fixed heat pipe geometry, Equation 10 may be written in terms of only fluid properties as

$$Q_{max} = K_1 \frac{\lambda \mu_\ell \rho_v}{\rho_\ell} \left\{ -K_2 + \left[K_2{}^2 - K_3 \left(K_4 \frac{\rho_\ell}{\sigma \cos \theta} - 1 \right) \frac{\sigma \rho_\ell{}^2 \cos \theta}{\rho_v \mu_\ell{}^2} \right]^{\frac{1}{2}} \right\}$$

where K_1, K_2, K_3, and K_4 are constants representing groups of fixed geometrical parameters. Thus, for large Q_{max}, Equation 10 shows that the following trends in fluid properties should exist:

- $\lambda \mu_\ell \rho_v / \rho_\ell$ should be large

- $\rho_\ell / \sigma \cos \theta$ should be small {the term $[(K_4 \rho_\ell / \sigma \cos \theta) - 1]$ must be negative}; this is significant only in a gravity field.

- $\sigma \rho_\ell{}^2 \cos \theta / \rho_v \mu_\ell{}^2$ should be large.

Since contradictions appear to exist in some properties of the three groupings above, it is impossible to set forth any one fluid property group that should be maximized. The only sure way to compare working fluids for a specified heat pipe geometry is to substitute their properties into Equation 10 and to note the trend in maximum power limit. This task was performed for some of the more promising working fluids considering the baseline geometrical constants listed in Table 1.

The results of the working fluid comparison are shown in Figure 11, where maximum heat transfer rate is plotted versus operating temperature for various fluids. It is seen that for high-temperature performance sodium appears to be a much better fluid than cesium. Other investigations (Refs. 5, 6, and 7) have shown potassium and lithium to be good high-temperature fluids also.

22
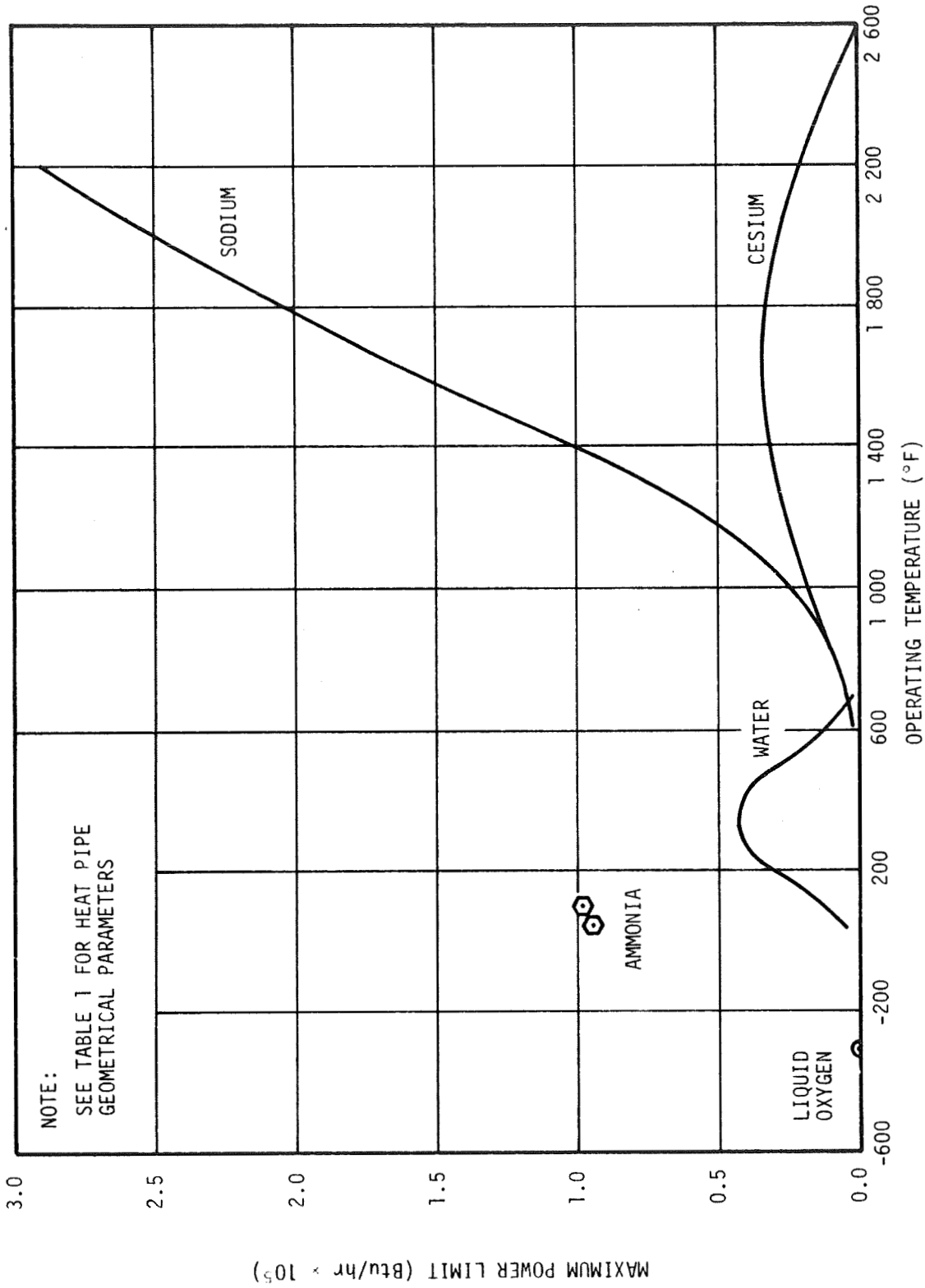
FIGURE 11. MAXIMUM POWER LIMIT AS A FUNCTION OF OPERATING TEMPERATURE FOR VARIOUS WORKING FLUIDS CONSIDERING FIXED HEAT PIPE GEOMETRY

23

For applications in the temperature range 50 to 600° F, water is about the best heat pipe fluid available. Reference 5 points out that water has an order of magnitude greater capacity than ethyl alcohol, and almost two orders of magnitude greater capacity than the Minnesota Mining Company fluid FC-78.

For applications at temperatures below the freezing point of water, but above - 100° F, ammonia is suitable. A lack of surface tension data prevented complete analysis of ammonia. Below - 100° F the cryogenic fluids are available. A calculation was performed for liquid oxygen at one temperature, as shown by Figure 11. Again, lack of surface tension data prevented complete evaluation.

Although only a few fluids were evaluated here, an optimum heat pipe design should include a similar evaluation of all available wetting fluids that have boiling points and saturation pressure which coincide with the desired operating range.

D. Wick Characterization

The wick, or capillary structure, is a vital component of the heat pipe. It must serve to pump the condensate from the cold end to the hot end with a minimum of internal resistance to the flow. These two requirements are contradictory, since the small pore size that is needed to effectively pump the liquid causes high internal resistance. Wick design configurations admit of wide variation. Wick types that have been investigated include wire screens, sintered metal fibers, woven glass fibers, fibrous paper, and axial grooves machined in the container wall with and without wire screen coverings.

Examination of Equation 10 shows that the pertinent properties that characterize wick structure relative to heat pipe usefulness are mean pore radius, r_c, fraction of wick volume occupied by the liquid (porosity), ϵ, and the dimensionless geometrical constant b. Desirable wick structures are characterized by large b and small ϵ and r_c.

The constant b is rather poorly defined in the literature as simply a "dimensionless goometrical constant". Reference 2 introduced the term b, and reported only that the nonconnected parallel cylindrical pores $b \approx 8$, and for wick structure with tortuous and interconnected passages

$b \approx 10$ to 20. Kemme (Ref. 4) referred to b as the "screen permeability factor" and reported a value of $b = 12$ for a screen having an effective radius, r_c, of 0.08 millimeters, thickness of 0.22 millimeters and porosity, ϵ, of 0.5. Evidently, b must be determined experimentally from liquid pressure drop measurements for each capillary structure of interest.

Since it is usually desirable to have a minimum temperature differential between the liquid-vapor interface and the container wall, it is important that the wick structure have a large thermal conductance. Reference 5 reported one test in which a heat pipe failed because of boiling between the pipe wall and a woven glass fiber wick. The vapor film apparently pushed the wick away from the wall, resulting in a burnout of the pipe. The failure occurred even at a low power input level of 40 watts. From this failure it was concluded by Reference 5 that

- The thermal conductivity of nonmetal wicks is too low for use in heat pipes designed for high power levels

- The wick structure should be bonded to the pipe wall to decrease the resistance to energy conduction.

Numerous tests (Refs. 1, 4, and 8 through 10) have demonstrated that wicks constructed of wire screens bonded to or press-fit against either grooved or nongrooved walls have sufficient thermal conductance to permit continuous operation at high power input levels without failure due to film boiling.

SECTION III. ANALYSIS OF HEAT PIPE APPLICATIONS TO SPACECRAFT THERMAL CONTROL PROBLEMS

After completion of a literature survey of heat pipe technology and the parametric analysis described above, some concepts were established which seemed to have obvious application to the solution of spacecraft thermal control problems. This section contains an analysis and discussion of each of the selected concepts. It is important to note that the applications cited here are only a few of the many heat pipe applications which can be expected to be discovered after subsystems are defined more clearly and designs progress further.

A. Utilization of Heat Pipe Concept to Control Boiloff Rate of Stored Cryogen

An application of the heat pipe concept which is potentially attractive consists of utilizing a closed heat pipe loop to absorb and reject excess heat leak through cryogenic tanks during extended storage in space. The concept is illustrated schematically in Figure 12. A sealed, continuous heat pipe loop is deployed such that one portion is in contact with the stored cryogen or tank walls inside the insulation. Another portion of the closed loop at the outer vehicle skin constitutes a radiator which is considered to be thermally shielded such that it radiates to deep space. The working fluid sealed inside the heat pipe is also a cryogen which has a boiling temperature slightly lower than that of the stored cryogen. The working fluid could possibly be the same type fluid as the stored cryogen, but at a slightly lower pressure.

As heat leaks through the normal insulation and is transmitted to the heat pipe in contact with the tank walls or stored cryogen, the working fluid in the heat pipe wick evaporates, absorbing its latent heat of phase change, at a lower temperature than the saturation temperature of the stored cryogen. The generated vapor flows at its saturation temperature to the cooler radiator end of the heat pipe because of the difference in vapor pressure, where it condenses onto the wick, giving up its latent heat. The condensate returns to the portion of the heat pipe in the storage tank by capillary pumping, where it is ready to absorb more heat through the vaporization process. If all of the heat leak could be transferred to the heat pipe, the boiloff rate would be reduced to zero. Since the heat pipe is not in contact with all of the tank wall or cryogen, only part of the heat leak will be absorbed, and the amount of boiloff
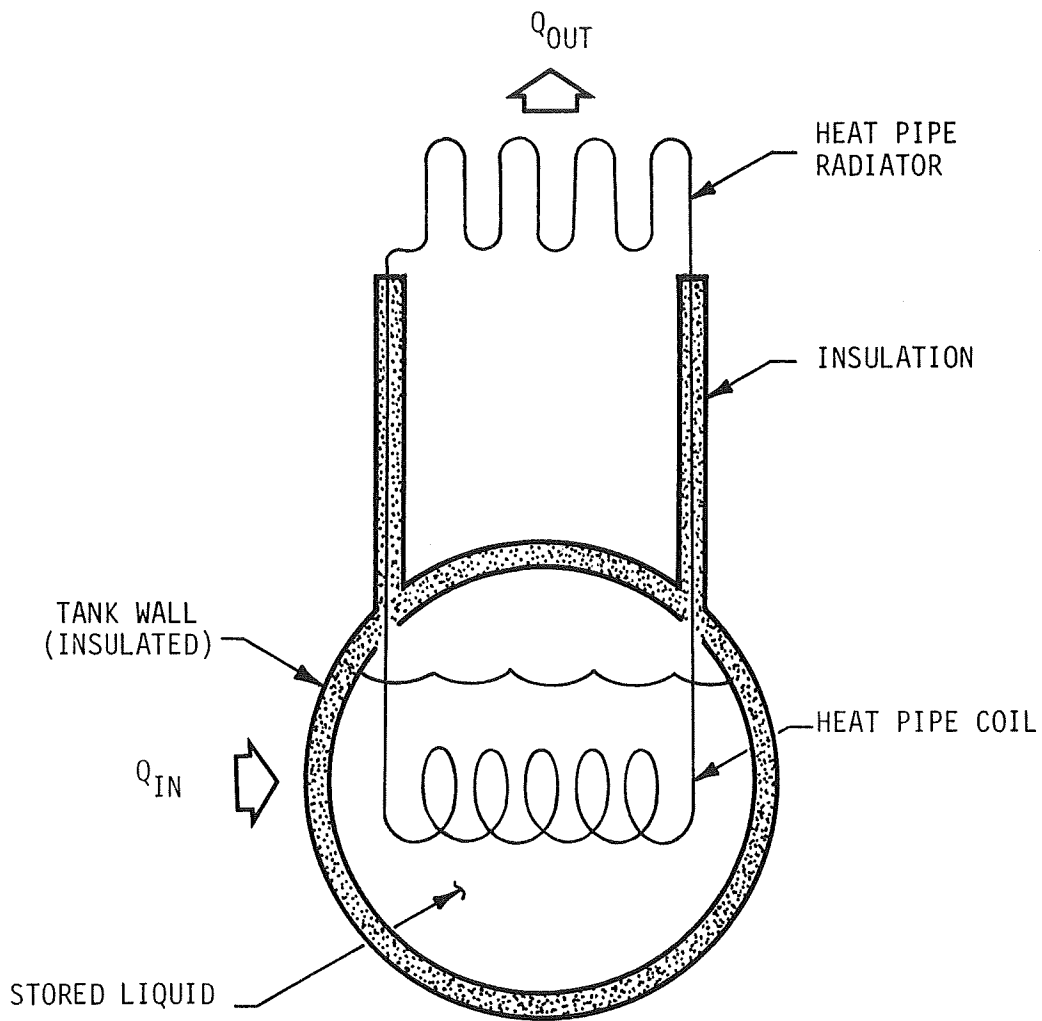
FIGURE 12. USE OF HEAT PIPE CONCEPT TO CONTROL STORED LIQUID TEMPERATURE
            OR BOILOFF RATE

reduction will depend on the degree of contact between the heat pipe and the stored cryogen. One method of improving the amount of contact would consist of utilizing a double-wall tank which is lined with a saturated wick. The space between the walls could then act as a vapor chamber (Ref. 11) and absorb the heat leak through the outer wall. By connecting the vapor chamber through a heat pipe loop to a radiator, as described above, the vapor could be condensed and returned through the wick to the vapor chamber by capillary pumping. The working fluid again would have a boiling temperature slightly lower than that of the stored cryogen to keep the temperature of the stored cryogen below its saturation temperature.

Application of this concept could result in a large weight savings if the duration of cryogenic storage is a long period. This is illustrated by Figure 13. Without the heat pipe boiloff reduction system, the excess weight at lift-off will consist of the weight of the predicted amount of liquid boiloff during the storage duration, plus the extra weight of the tanks required to contain the boiloff. With the heat pipe boiloff reduction system, the excess weight at lift-off will consist of the weight of the heat pipe system, including the heat pipe radiator, plus the weight of the reduced amount of boiloff. If all the heat leak through the tank insulation could be transferred to the heat pipe loop, the boiloff would be reduced to zero. The realizable weight savings increases with desired duration of cryogen storage, as shown in Figure 13. For short missions, it may be more advantageous to simply haul extra liquid and to tolerate some boiloff. However, for long storage durations, the expected boiloff weight is excessive.

Hopefully, the heat pipe system will provide a significant weight savings. However, a thorough systems study is required to provide meaningful numerical results. Such a thorough study is not within the scope of this work and should be conducted as a separate follow-on study.

As a first step to determining the technical feasibility of this concept, the maximum limiting heat flux that could be radiated by the radiator end of the loop was calculated for some candidate cryogenic working fluids. Fluids considered were liquid oxygen, nitrogen, fluoride, neon, hydrogen, and helium. The maximum limiting heat flux from the radiator was calculated from the Stefan-Boltzmann relation

$$q_{max} = \sigma \epsilon T^4 \tag{14}$$
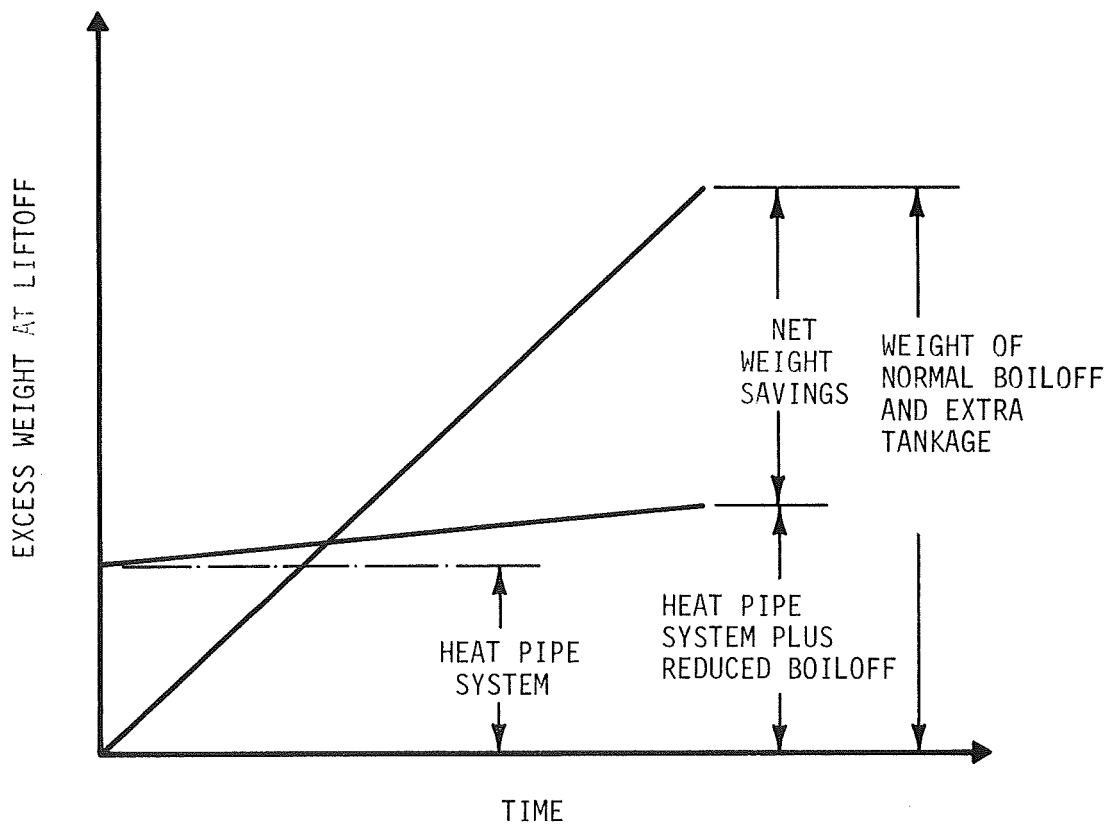
FIGURE 13. POTENTIAL WEIGHT SAVINGS PROVIDED BY HEAT PIPE
BOILOFF REDUCTION SYSTEM

where

q_{max} - maximum limiting radiator heat flux, $Btu/hr\text{-}ft^2$

σ - Stefan-Boltzmann constant, 0.1718×10^{-8} $Btu/hr\text{-}ft^2\text{-}°R^4$

T - absolute temperature of radiating surface, $°R$

ϵ - surface emissivity.

Utilization of this equation assumes radiation from a surface at temperature, T, and emissivity, ϵ, to deep space at $0°R$. It is noted that for the concept considered here to be successful, the radiator must be shielded such that irradiation is practically zero.

The calculated maximum limiting heat flux is plotted as a function of radiator surface temperature in Figure 14, assuming a surface emissivity of 0.9. Also noted on Figure 14 are the saturation temperatures of the six cryogenic fluids (at a pressure of 14.7 psia) and the corresponding maximum heat flux values that could be attained by a radiator at these temperatures. Thus, if a radiator with surface emissivity of 0.9 were constructed using liquid oxygen at 14.7 psia as the working fluid, and if this radiator could be made of 100-percent efficient with its entire surface at the saturation temperature of 162.4°R, the maximum attainable radiation heat flux would be 1.085 $Btu/hr\text{-}ft^2$. Of course, various deficiencies prevent the attainment of this maximum radiation flux. However, it is also noted that typical values of heat leak flux through insulated cryogenic tank walls are of the order 0.2 $Btu/hr\text{-}ft^2$. Therefore, it is possible that the ratio of radiator surface area to storage tank surface area could be appreciably less than unity, and the concept approaches practicality. The concept could also be enhanced by utilizing a highly efficient radiator constructed entirely of heat pipes, as discussed by Reference 6.

It is important to note that the maximum limiting radiation flux for a heat pipe radiator employing hydrogen, helium, or neon as the working fluid is extremely small, because of their low boiling temperatures. This observation essentially eliminates this concept as a boiloff reduction system for liquid hydrogen because the heat pipe fluid saturation temperature which is assumed to be the radiator temperature must be even lower than that of the stored cryogen. Therefore, the ratio of
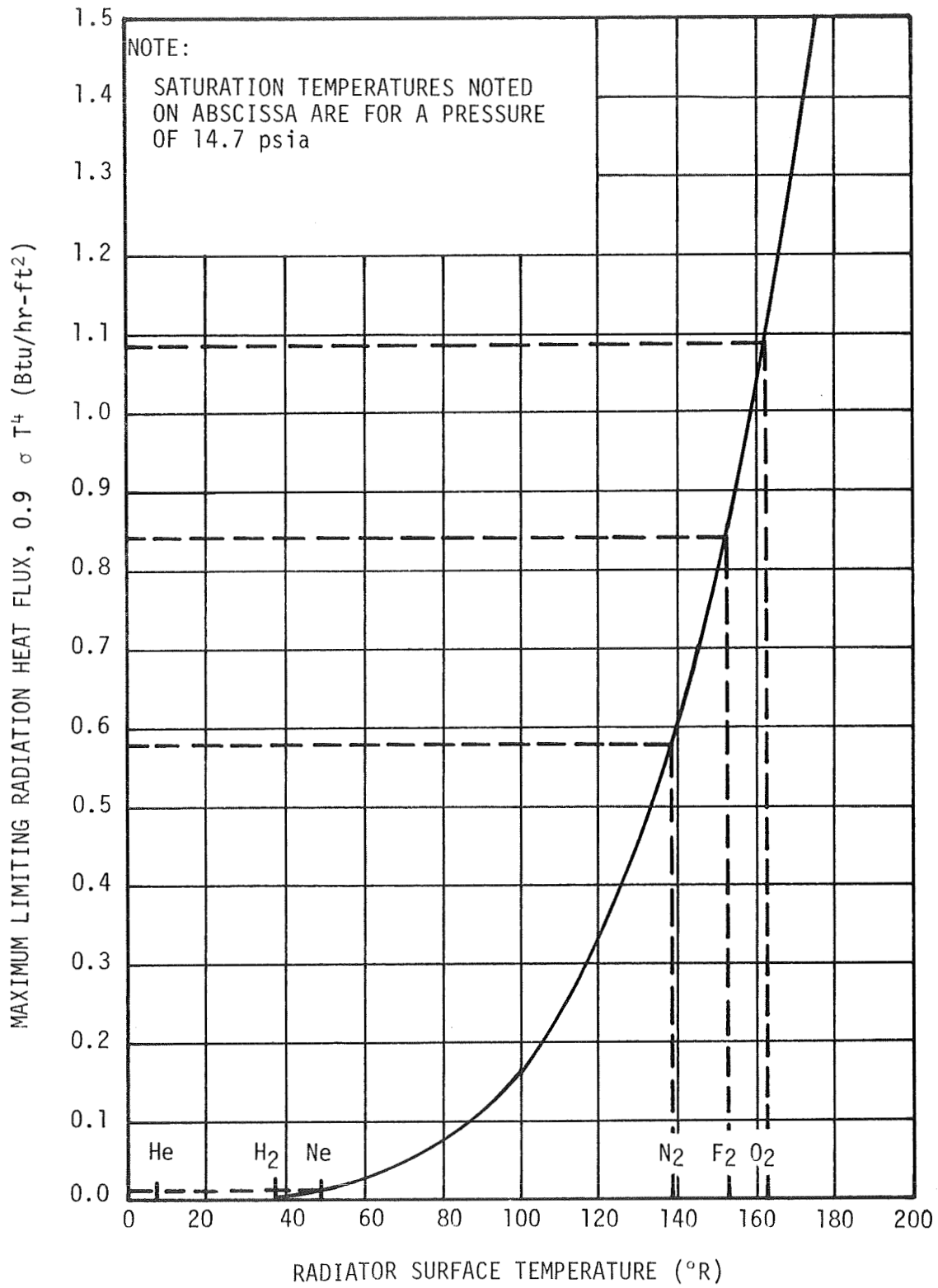
FIGURE 14. MAXIMUM LIMITING RADIATION HEAT FLUX AS A FUNCTION
OF RADIATOR SURFACE TEMPERATURE

32

radiator to storage tank area would be extremely large (≈ 100), and the concept would be feasible for only very small tanks. However, the concept does appear more promising for liquid oxygen.

To permit estimation of the minimum radiator areas that would be required to reject various heat leak fluxes using LO_2 or LN_2 as the heat pipe working fluid, Figure 15 was prepared. It shows the minimum ratio of radiator to tank surface area versus average heat leak flux through the tank wall. The actual radiator surface area will always be somewhat greater than indicated by this ratio. To obtain the curves of Figure 15, it was assumed that all heat leak through the tank insulation is transferred through the heat pipe loop to the radiator. Each value represented by these curves is simply the ratio of the tank heat leak flux in question to the maximum limiting radiator heat flux shown by Figure 14 for the respective working fluids. It is noted from Figure 15 that for typical heat leak fluxes of about 0.2 Btu/hr-ft^2, the minimum possible ratios of radiator to tank surface area are 0.35 for LN_2 and 0.175 for LO_2. These small ratios indicate that the concept could be successful utilizing radiators of reasonable dimensions.

If higher heat pipe working fluid pressures are permissible, increased heat rejection potential is available because of increased working fluid saturation temperature and, hence, increased radiator surface temperature. The effect of increased heat pipe pressure on maximum limiting radiator heat flux is illustrated by Figure 16 for LO_2 and LN_2.

Perhaps the most difficult problem to overcome in achieving feasibility in this concept is that of thermally shielding the radiator portion of the heat pipe loop from heat gains due to conduction through the spacecraft structure and irradiation from the spacecraft and external (solar, albedo, or planetshine) sources. Since the radiator must function at cryogenic temperatures, heat gain from sources other than the cryogenic storage tank must be almost completely eliminated. Otherwise, the radiator would simply act as a heat collector, and the heat pipe loop would function in reverse to add more heat to the storage tank.

One method of reducing unwanted irradiation from solar, albedo, and planetshine sources for an Earth-orbital vehicle is to orient the spacecraft judiciously during flight. For example, by orienting the vehicle broadside to the Earth, as shown by Figure 17, with the radiator
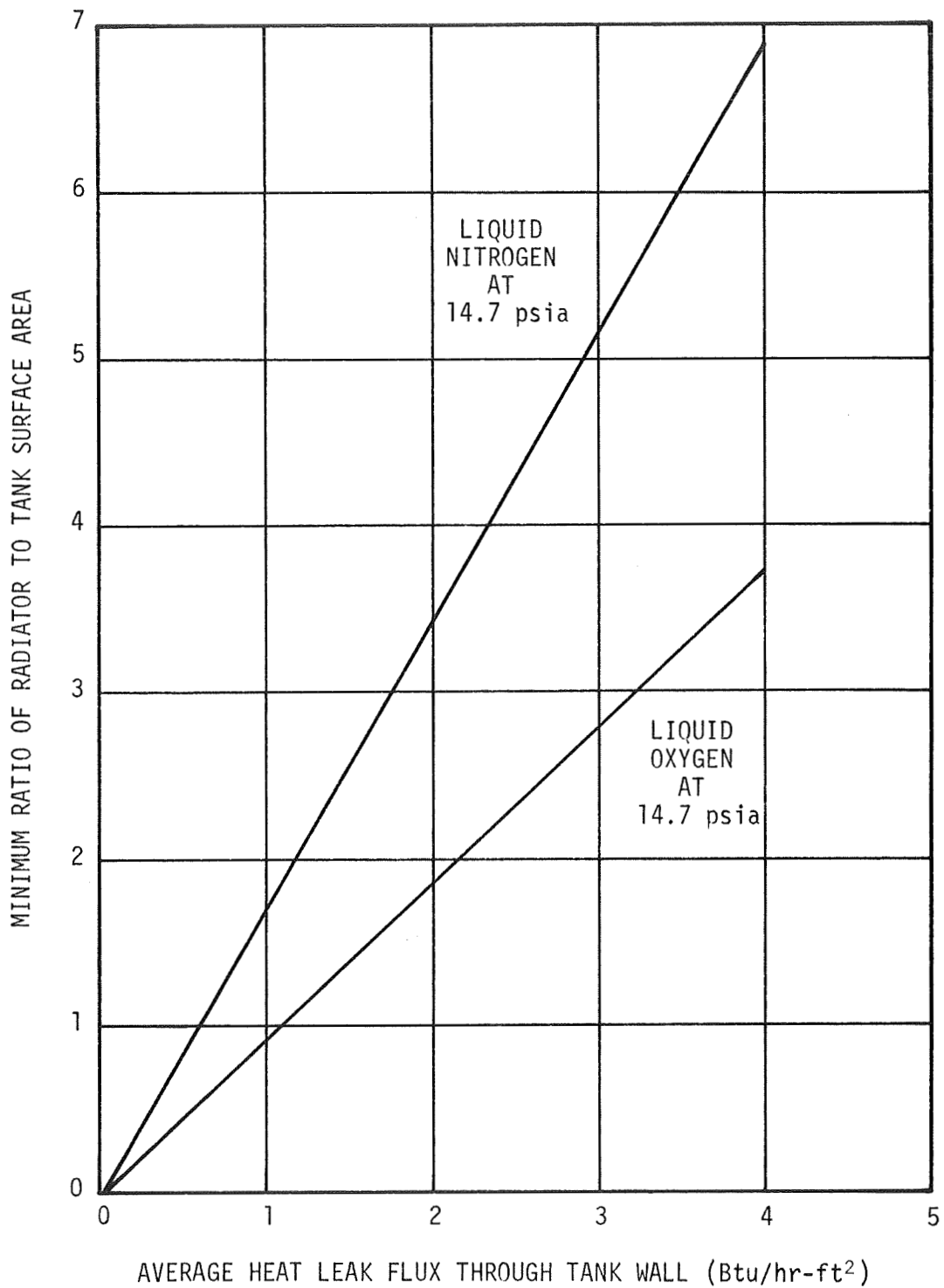
FIGURE 15. MINIMUM RATIO OF RADIATOR TO TANK SURFACE AREA AS A FUNCTION
OF AVERAGE HEAT LEAK FLUID THROUGH TANK WALL
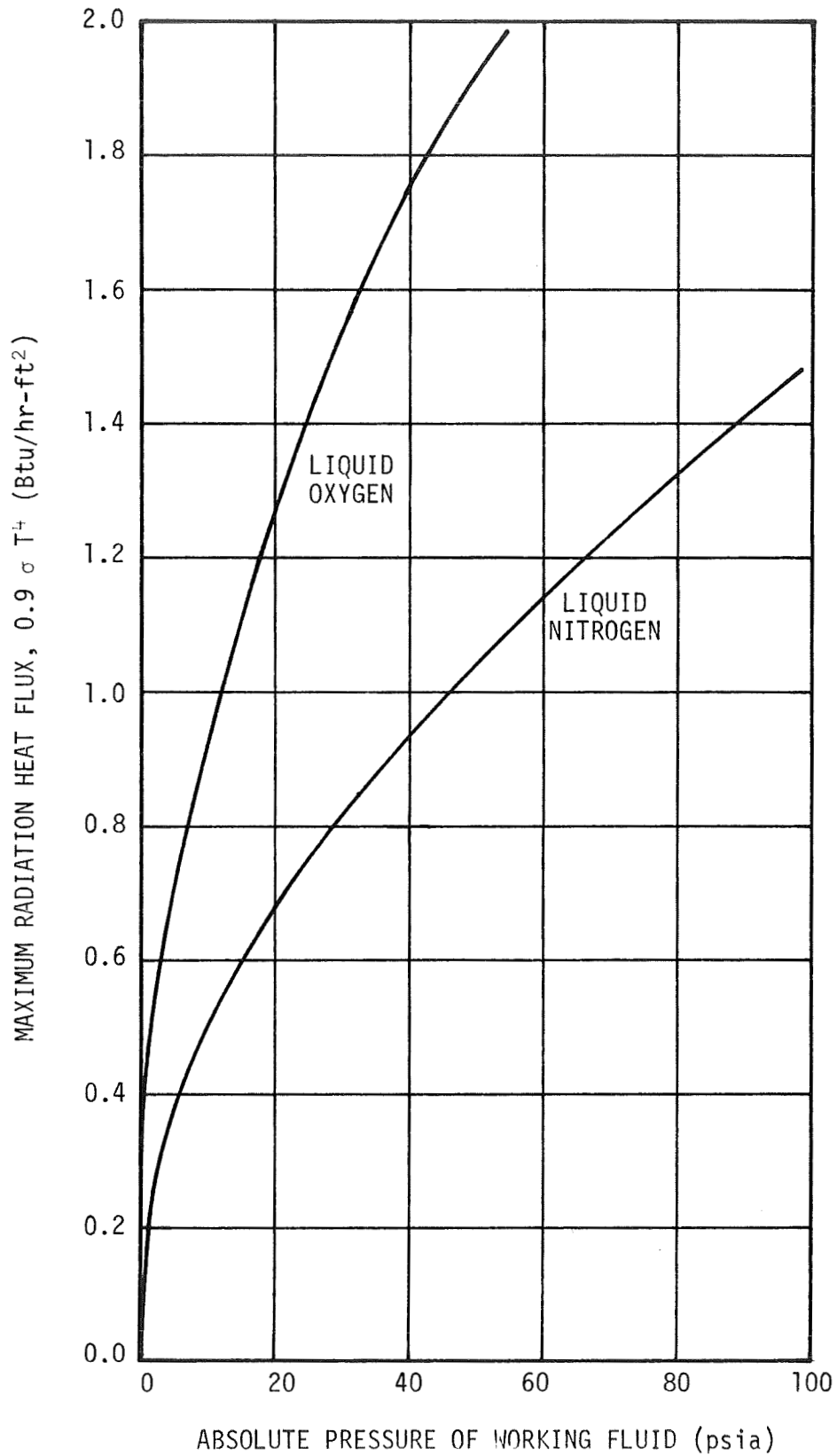
FIGURE 16.   MAXIMUM RADIATION HEAT FLUX AS A FUNCTION
OF HEAT PIPE WORKING FLUID PRESSURE FOR
LO_2 AND LN_2

35
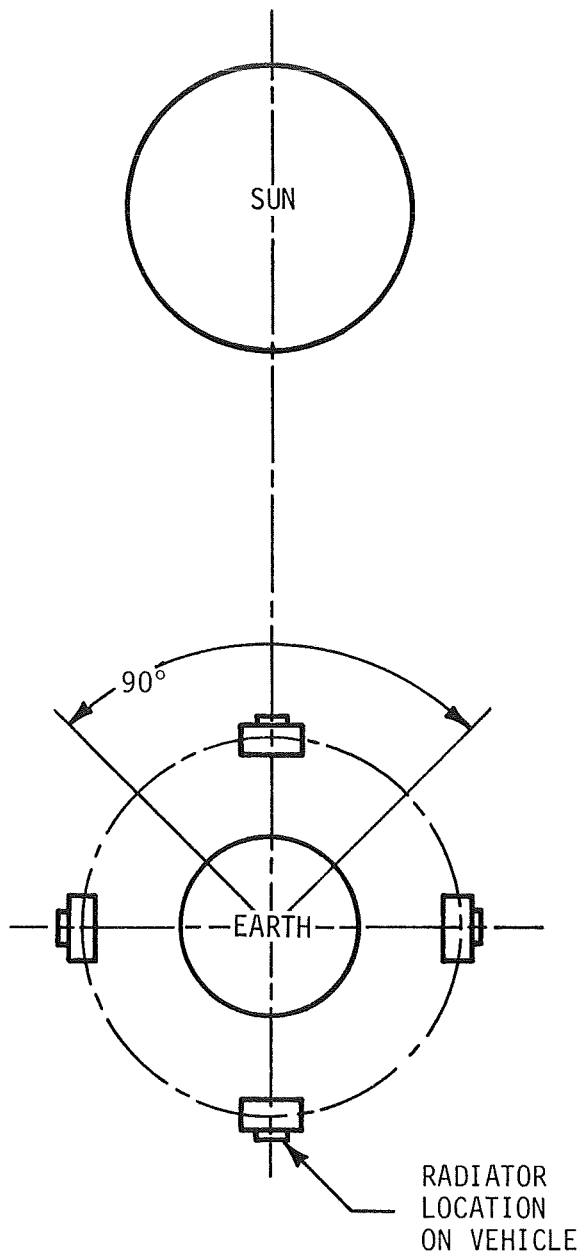
FIGURE 17.   ILLUSTRATION OF METHOD TO REDUCE IRRADIATION TO RADIATOR
             BY PROPER VEHICLE ORIENTATION

directed away from the Earth, external irradiation is essentially zero during three-fourths of the orbit. During the remaining one-fourth of the orbit, the radiator receives direct radiation from the Sun. During this period of maximum irradiation, a means must be provided to prevent reverse operation of the heat pipe loop such that more heat is not added to the storage tank. This might be accomplished by shading the radiator using louvers or some such device, and/or by "killing" the heat pipe operation temporarily, thus blocking the flow of vaporized working fluid to the portion of the loop in contact with the stored cryogen. Vapor flow in the heat pipe loop could be blocked temporarily by allowing a noncondensible gas (e. g., helium) to escape from a pressurized vessel and to flow into the portion of the heat pipe loop in contact with the stored liquid. The noncondensible gas would remain in the cooler end of the heat pipe, as demonstrated by Reference 1 and other experiments, throughout the period of maximum irradiation. As the vehicle moves out of the region of high irradiation, the noncondensible gases would be withdrawn again into the second vessel, thus allowing the heat pipe loop to function normally again. Obviously, some method would have to be provided for ensuring withdrawal of only noncondensible gases and no working fluid.

The concept discussed here for reducing liquid boiloff during long-term cryogenic storage appears to have considerable potential. It is particularly attractive because it is simple, self-contained, and requires no mechanical pumps or other hardware which are susceptible to failure. Of course, obstacles may arise which will challenge the technical feasibility of the concept. For example, Reference 5 states that cryogenic fluids are relatively poor heat pipe working fluids. They may be adequate, however, to reject the small heat leak rates through insulated tanks. It is felt that the idea warrants careful consideration and further investigation to provide a conclusive evaluation of its worth.

B. Thermal Analysis of Heat Pipes Integrated into Spacecraft Skin to Improve Temperature Uniformity

Heat pipes may have an application in improving the temperature uniformity of the outer surface of an object, such as a spacecraft, which is subjected to nonuniform heating from an external source. For this discussion consider a long metal cylinder which is subjected to combined solar, albedo, and planetshine irradiation. Without heat pipes the skin temperature will obviously be nonuniform around the vehicle because of nonuniform heating. The addition of heat pipes around the circumference

at regular axial intervals (see Figure 18) will cause almost immediate transfer of heat received by the heat pipes from irradiated areas around to the shaded areas with practically no temperature drop. This creates a series of narrow isothermal bands around the vehicle, and the only variation in temperature is between each heat pipe and the adjacent metal. Thus, heat conduction around the cylinder may be neglected, and the only appreciable heat flow in the metal skin will be axially between the heat pipe and the adjacent metal.

The differential equation describing the heat flow in the metal between heat pipes may be derived as follows.

Consider the cylindrical segment illustrated in Figure 19 as the model for analysis. The derivation is based on the following assumptions:

- Heat flow by conduction in the skin is in the axial direction only (radial and circumferential temperature gradients are negligible).

- The inside surface of the vehicle skin is adiabatic.

- The total absorbed irradiation flux, Q_s, including solar, albedo, and planetshine components, is known.

- Thermophysical properties of the skin structure are invariant with temperature.

- Heat transfer is steady state.

Based on the above assumptions, the appropriate heat balance equation is as follows:

$$\boxed{\begin{array}{c}\text{Conduction into}\\ \text{Element dx at x}\end{array}} + \boxed{\begin{array}{c}\text{Total Absorbed}\\ \text{Irradiation}\\ \text{Between x and}\\ \text{(x + dx)}\end{array}} = \boxed{\begin{array}{c}\text{Conduction out}\\ \text{of Element dx}\\ \text{at (x + dx)}\end{array}} + \boxed{\begin{array}{c}\text{Infrared Radiation}\\ \text{from Element dx}\\ \text{Between x and}\\ \text{(x + dx)}\end{array}} \qquad (15)$$

Expressed mathematically this heat balance becomes

$$- k_s (2 \pi \bar{r} \delta) \frac{dT}{dx}\bigg|_x + Q_s (2 \pi r_o dx) = - k_s (2 \pi \bar{r} \delta) \frac{dT}{dx}\bigg|_{x+dx}$$

$$+ \sigma \epsilon (2 \pi r_o dx) T^4 \qquad (16)$$

38
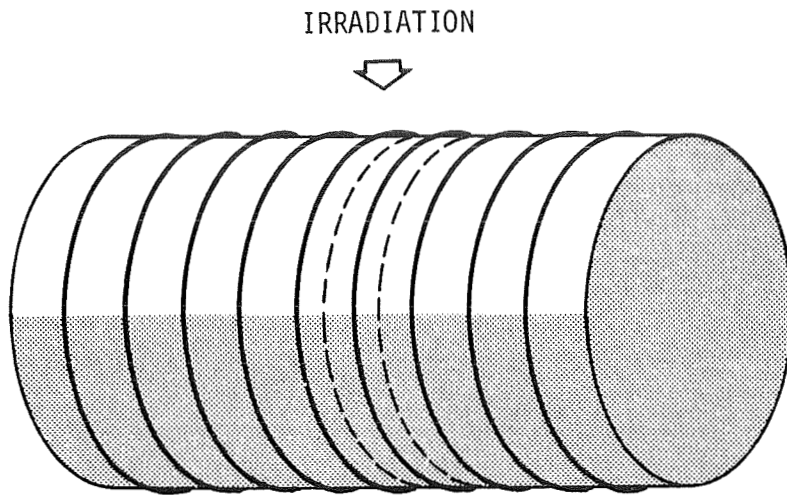
IRRADIATION

FIGURE 18. SCHEMATIC OF IRRADIATED CYLINDRICAL SPACECRAFT
WITH HEAT PIPES ATTACHED TO OUTER SKIN
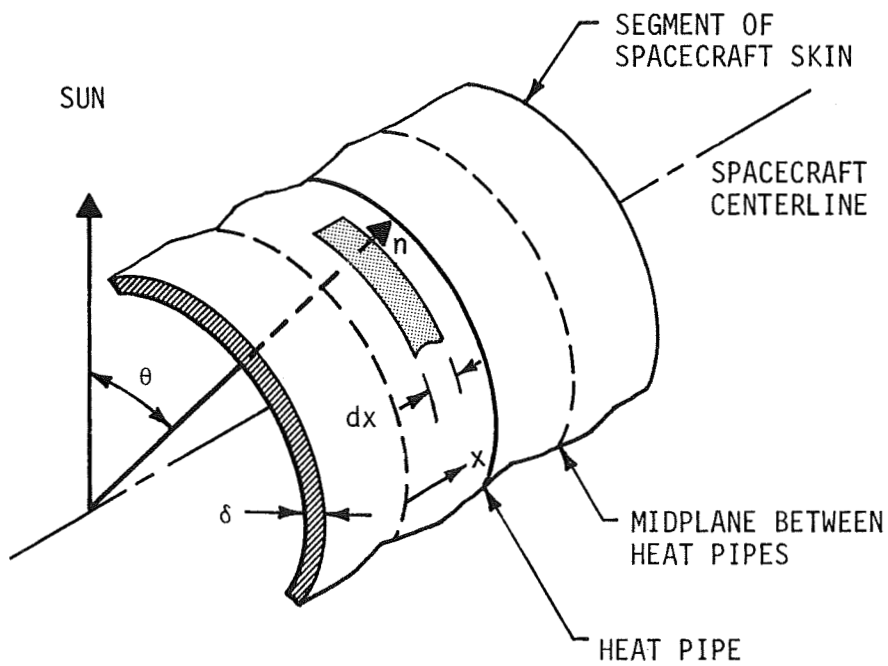
FIGURE 19. MATHEMATICAL MODEL FOR ANALYSIS OF HEAT PIPES
INTEGRATED INTO SPACECRAFT SKIN

where

k_s -   thermal conductivity of spacecraft skin material, Btu/hr-ft-°R

$\bar{r}$ -   mean radius of outer skin, ft

δ -   skin thickness, ft

T -   local skin temperature, °R

x -   axial distance from station midway between heat pipes, ft

Q_s -   local total absorbed irradiation flux, including solar, albedo, and planetshine, Btu/hr-ft^2

r_o -   radius of outer skin surface, ft

σ -   Stefan-Boltzmann constant, 0.1718×10^{-8} Btu/hr-ft^2-°R^4

ϵ -   emissivity of outer skin surface.

For cylinders of large radius, $\bar{r} \approx r_o$; and the equation above may be reduced to the following differential equation with the aid of the mean value theorem:

$$- k_s \, \delta \left. \frac{dT}{dx} \right|_x + Q_s \, dx = - k_s \, \delta \left\{ \left. \frac{dT}{dx} \right|_x + \left[\frac{d}{dx} \left(\frac{dT}{dx} \right) \bigg|_M \right] dx \right\}$$

$$+ \, \sigma \, \delta \, T^4 \, dx$$

where M is located somewhere between x and (x + dx). The terms

$$- k_s \, \delta \left. \frac{dT}{dx} \right|_x$$

cancel, and as the size of the element approaches zero as a limit, a value at M becomes a value at the point x. Thus, further reduction yields the final form of the differential equation governing the heat flow:

$$\frac{d^2 T}{dx^2} = \frac{\sigma \epsilon}{k_s \, \delta} \, T^4 - \frac{Q_s}{k_s} \tag{18}$$

40

or

$$\frac{d^2 T}{dx^2} = a + b\, T^4 \qquad (19)$$

where

$$a = -\frac{Q_s}{k_s \delta}$$

$$b = \frac{\sigma \epsilon}{k_s \delta} \; .$$

The applicable boundary conditions are

- $\left(\dfrac{dT}{dx}\right)_{x=0} = 0$

    or the temperature midway between heat pipes represents either the minimum or maximum for each circumferential location, with no axial heat conduction at this point.

- $T_{x = B/2}$

    is the same for each element, since it is the heat pipe temperature (B is the heat pipe spacing).

- $\displaystyle\int_0^{2\pi} \left(\dfrac{dT}{dx}\bigg|_{x = B/2}\right) d\theta = 0.$

    This condition specifies that the net heat flow into the heat pipe by conduction equals the net heat flow out of it, around the cylinder.

By letting

$$y = \frac{dT}{dx} \quad , \qquad (20a)$$

and

$$\frac{d^2 T}{dx^2} = y \frac{dy}{dT} \qquad (20b)$$

41

Equation 19 may be integrated to yield

$$\frac{dT}{dx} = \left(2\,a\,T + \frac{2}{5}\,T^5 + c \right)^{\frac{1}{2}} \tag{21}$$

Applying the condition $T = T_o$, $dT/dx = 0$ at $x = 0$, the following relation is obtained

$$\frac{dT}{dx} = \left[\frac{2}{5}\,b\,(T^5 - T_o^5) + 2\,a\,(T - T_o) \right]^{\frac{1}{2}} \tag{22}$$

where T_o is the temperature midway between heat pipes.

Following the procedure of Reference 11, the temperature between heat pipes may be calculated approximately from a truncated MacLaurin series

$$T = T_o + \frac{x^2}{2} \left(\frac{d^2 T}{dx^2} \right)_{x=0} + \frac{x^4}{24} \left(\frac{d^4 T}{dx^4} \right)_{x=0} + \frac{x^6}{720} \left(\frac{d^6 T}{dx^6} \right)_{x=0} \tag{23}$$

where $\left(\dfrac{d^2 T}{dx^2} \right)_{x=0}$

is given by Equation 18 with T set equal to T_o, and the higher derivatives are found by repeated differentiation of $d^2 T/dx^2$, noting that

$$\left(\frac{dT}{dx} \right)_{x=0} = 0 \quad .$$

Thus,

$$\left(\frac{d^4 T}{dx^4} \right)_{x=0} = 4\,b\,T_o^3 \left(\frac{d^2 T}{dx^2} \right)_{x=0} \tag{24}$$

and

$$\left(\frac{d^6 T}{dx^6} \right)_{x=0} = 36\,b\,T_o^2 \left(\frac{d^2 T}{dx^2} \right)_{x=0}^2 + 4\,b\,T_o^3 \left(\frac{d^4 T}{dx^4} \right)_{x=0} \quad . \tag{25}$$

42

The computational procedure for determining the temperature distribution between heat pipes around the cylinder is described below.

It is assumed that the heat pipe spacing, B, the total absorbed irradiation flux variation around the vehicle, Q_s, the skin thickness, δ, and thermophysical properties are given. The step-by-step computational procedure then is as follows:

(1) Assume a value of temperature, T_o, midway between heat pipes at $\theta = 0$, where θ is circumferential angle from an arbitrary starting point on the cylinder.

(2) Calculate the heat pipe temperature, $T_{B/2}$, at $\theta = 0$ from Equation 23 based on T_o and the appropriate value of Q_s.

(3) Calculate the slope

$$\left(\frac{dT}{dx}\right)_{x = B/2}$$

at the heat pipe from Equation 22.

(4) Increment θ, assume a value of T_o at this angle (a good guess would be T_o for the last increment).

(5) Calculate the heat pipe tmeperature, $T_{B/2}$, at the new θ based on the assumed T_o and the appropriate value of Q_s at the new θ.

(6) If the value of heat pipe temperature calculated in Step 5 equals the value established in Step 2 (within specified limits), go to Step 7. If not equal, make new estimate of T_o, return to Step 5.

(7) Calculate the slope

$$\left(\frac{dT}{dx}\right)_{x = B/2}$$

at the current value of θ.

(8) If $\theta \leq 2\pi$, go back to Step 4. If $\theta \geq 2\pi$, go to Step 9.

(9) Evaluate $\int_0^{2\pi} \left(\dfrac{dT}{dx}\right)_{x = B/2} d\theta$ numerically.

(10) If value of integral calculated in Step 9 equals zero (within specified limits), the correct temperature distribution has been determined. If not equal, select new value of T_0 at $\theta = 0$, return to Step 2.

The procedure described above should be readily adaptable to solution on the digital computer to permit rapid calculations. The results of a sample calculation by Reference 11 for a specified configuration demonstrated the effectiveness of heat pipes in improving the temperature uniformity of an irradiated surface.

C. Removal of Heat from a Concentrated Source Using the Heat Pipe

One important application of the heat pipe is to transport heat between a concentrated source, such as an electronic component, and a sink, such as a heat exchanger or radiator. The configuration considered in this analysis is shown in Figure 20. A cylindrical heat pipe is attached to a heat source at one end and a heat sink at the other end. Heat enters the heat pipe by axial conduction into the pipe walls at the source end and leaves by the same mechanism at the sink end. The pipe is considered to be perfectly insulated with no heat loss between the ends. Heat flows axially through the pipe walls by conduction and radially through the liquid-saturated wick by evaporation, condensation, and conduction.

The following assumptions are utilized in the analysis:

● Heat transfer is considered to be steady state.

● Pipe wall thermophysical properties are invariant with temperature.

● The pipe wall temperature varies only in the axial direction.

● The outer surface of the heat pipe is perfectly insulated.
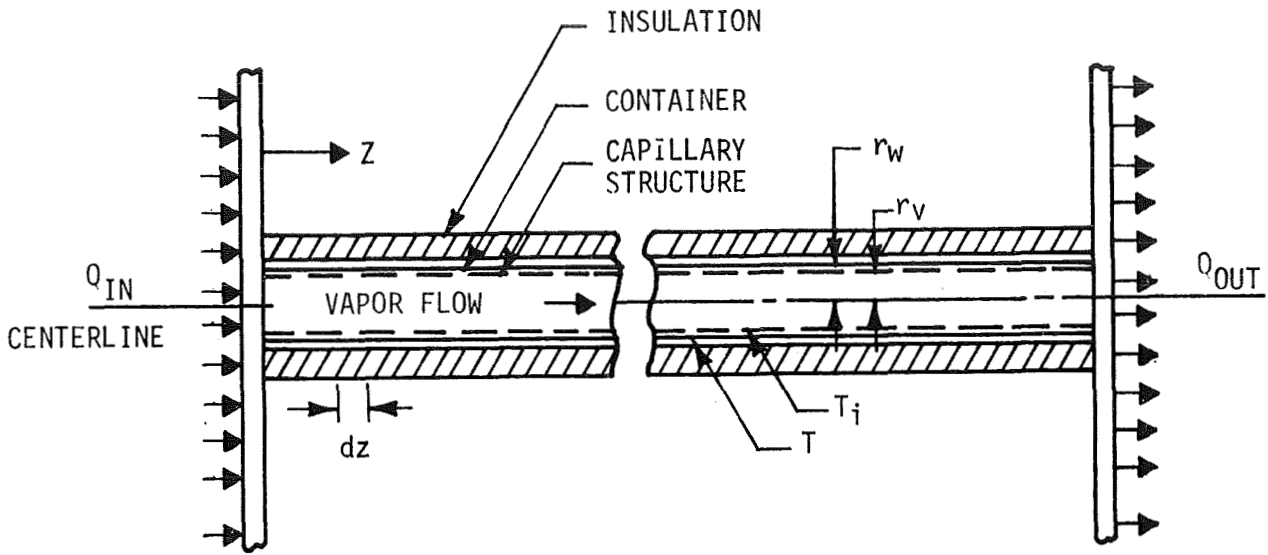
FIGURE 20. SCHEMATIC OF HEAT PIPE BETWEEN SOURCE AND SINK

Considering an axial element dz of pipe wall from Figure 20, the following heat balance may be written for steady-state heat transfer:

$$
\boxed{\begin{array}{c}\text{Axial Conduction}\\ \text{into Element}\\ \text{at z}\end{array}} \quad - \quad \boxed{\begin{array}{c}\text{Axial Conduction}\\ \text{out of Element}\\ \text{at (z + dz)}\end{array}} = \boxed{\begin{array}{c}\text{Radial Heat Transfer}\\ \text{Through Wick Between}\\ \text{z and (z + dz)}\end{array}} \qquad (26)
$$

For the configuration shown by Figure 20, the applicable equation is

$$
- k_p A_c \left.\frac{dT}{dz}\right|_z - \left[- k_p A_c \frac{dT}{dz}\bigg|_z - \frac{d}{dz}\left(k_p A_c \frac{dT}{dz}\right)\bigg|_M \Delta z \right]
$$

$$
= h P \Delta z (T - T_i) \qquad (27)
$$

where

    T - temperature of pipe wall, °R

    T_i - temperature at liquid-vapor interface, °R

z -   axial distance from end of heat pipe, ft

k_p -   thermal conductivity of pipe wall, Btu/hr-ft-°R

A_c -   cross sectional area of heat pipe wall, ft^2

P -   perimeter of container at inside surface, ft

h -   average heat transfer coefficient, Btu/hr-ft^2-°R.

The product p dz represents the surface area of the pipe wall between sections z and (z + dz) in contact with the working fluid. The terms $\left(k_p A_c \, dT/dz \mid z \right)$ cancel, and as the size of the element approaches zero as a limit, a value at M becomes a value at the point X. The differential equation may then be reduced to

$$\frac{d^2 T}{dz^2} = m^2 \left(T - T_i \right) \tag{28}$$

where $\quad m = \left(\dfrac{hP}{k_p A_c} \right)^{\frac{1}{2}}$.

Equation 28 is a linear, second order, homogeneous differential equation with constant coefficients, whose general solution is

$$T - T_1 = c_1 \exp (mz) + c_2 \exp (-mz). \tag{29}$$

The largest variation in wall temperature will occur near the ends of the heat pipe. If the analysis is limited to the areas near the ends of the pipe where most of the evaporation and condensation occur, the appropriate boundary conditions are

$$\left[\quad \text{at:} \quad z = 0 \quad Q = -k_p A_c \left. \frac{dT}{dz} \right|_{z = 0} \quad \right] \tag{30a}$$

$$\left[\quad\quad z \rightarrow \infty, \quad T \rightarrow T_i \quad\quad \right] \tag{30b}$$

where z is now considered to be the distance from the appropriate (evaporator or condenser) end of the heat pipe. At the evaporator end,

46

Q is positive, and at the condenser end, Q is negative. The latter boundary condition is approximate, but is fairly realistic since most of the temperature variation occurs very near (within 1 to 2 inches) of the ends of the heat pipe.

Applying these boundary conditions to the general solution (Equation 29), the following particular solution is obtained for the temperature distribution along the heat pipe walls near the ends:

$$T - T_i = \frac{Q}{k_p A_c m} \exp(-mz) . \qquad (31)$$

The coefficient $(Q/k_p A_c m)$ will be positive at the evaporator end and negative at the condenser end. Also, the heat transfer coefficient, h, will be the boiling coefficient, h_b, at the evaporator end and the condensation coefficient, h_c, at the condenser end.

1. Evaluation of Heat Transfer Coefficients. Before Equation 31 can be solved for a particular problem, the boiling and condensation heat transfer coefficients, h_b and h_c, must be evaluated. The current state of knowledge of boiling and condensing heat transfer for wicked surfaces is very primitive. The information available with respect to spacecraft applications of heat pipes has two basic weaknesses. First, almost all of the heat transfer coefficients that have been measured are for conventional, unwicked surfaces. Second, very little data have been collected in 0-g acceleration fields. Therefore, any attempts to evaluate, h_b and h_c must, at present, be considered only approximate. Since it is desirable to be able to predict heat pipe engineering performance, relations will be presented for estimating h_b and h_c based on the 1-g information available to date. These relations are only tentative, and should be replaced as improved data becomes available.

The relative importance of gravitational and surface tension effects appears to be determined by the ratio of liquid volume to wetted surface area. In wick boiling and condensation, the liquid volumes in the capillary passages are small, and the ratio of surface area to liquid volume is large. Therefore, it is reasonable to expect that boiling and condensation in capillary structures are influenced primarily by surface tension forces, and that gravitational effects are of minor importance. If this hypothesis is correct, heat transfer data measured from capillary structures in the 1-g environment should be reasonably accurate for the 0-g environment.

47

a. Boiling Heat Transfer Coefficient. The recommended equation (Ref. 12) for estimating the boiling heat transfer coefficient, h_b, is

$$h_b = 0.072 \left(\frac{D_e\, G'}{\mu_\ell}\right)^{-0.77} \left(Pr_\ell\right)^{-0.6} \left(\frac{\rho_\ell\, \sigma\, g}{p^2\, g_c}\right)^{-0.21} c_{p_\ell}\, G' \quad (32)$$

where

h_b — average boiling heat transfer coefficient, $Btu/hr\text{-}ft^2\text{-}°R$

μ_ℓ — dynamic viscosity of liquid, $lbm/hr\text{-}ft$

Pr_ℓ — Prandtl number of liquid

D_e — dimension parameter, ft

G' — mass flux of liquid $\left(\dfrac{Q_e}{A_b\, \epsilon\, \lambda}\right)$, $lbf/hr\text{-}ft^2$

ρ_ℓ — density of liquid, lbm/ft^3

σ — surface tension of liquid-vapor-wick interface, lbf/ft

g — acceleration of gravity, ft/hr^2

g_c — dimensional constant, $lbm\text{-}ft/lbf\text{-}hr^2$

p — absolute pressure of liquid, lbf/ft^2

c_{p_ℓ} — specific heat of liquid, $Btu/lbm\text{-}°R$

A_b — area of boiling heat transfer surface, ft^2

ϵ — porosity of capillary structure

λ — latent heat of vaporization of liquid, Btu/lbm

Q_e — rate of heat transfer into evaporator, $Btu/hr.$

48

Until improved data are available for reduced gravity fields, the gravitational acceleration should be entered as 1-g. For a meshed fiber type capillary structure (wick), Reference 12 recommends that the dimensional parameter, D_e, be represented by

$$D_e = 4 r_h \tag{33}$$

where r_h is hydraulic radius. The hydraulic radius of this type of wick is defined as

$$r_h = \frac{\epsilon}{A_s} \tag{34}$$

where A_s is fiber surface area per unit volume of wick in ft^2/ft^3. The value of A_s may be calculated from

$$A_s = \frac{4 \rho_{w_i}}{\rho_f D_f} \tag{35}$$

where

ρ_{w_i} - density of fiber-void mesh, lbm/ft^3

ρ_f - fiber density, lbm/ft^3

D_f - mean fiber diameter, ft.

One difficulty which arises in evaluating h_b for the configuration of Figure 20 is that the surface area, A_b, over which boiling occurs is not known a priori. As heat is added to the end of the pipe and flows down the pipe walls and through the wick, evaporation will occur along an unknown distance down the heat pipe. This distance is required in evaluating the surface area, A_b, to be used ultimately in calculating G'; the average liquid mass flux through the capillary structure. One approach is to use a trial and error procedure in which the length of evaporation is first assumed to permit a trial calculation of h_b. This trial value is then used in Equation 31 to calculate the wall temperature distribution along the heat pipe. The evaporator length for the next iteration is determined as the distance at which the calculated wall temperature equals the liquid saturation temperature. However, one of the assumptions set forth in deriving Equation 31 was that the wall temperature approaches the liquid interface temperature as distance from the

end becomes infinite. Thus, the calculated wall temperature from Equation 31 will always be slightly greater than the desired liquid interface temperature even at large X. However, physical reasoning requires that the wall temperature must become less than the interface temperature at some point along the heat pipe, since condensation must begin. Since most of the evaporation occurs near the hot end of the pipe, the required evaporator length for evaluating h_b may be determined with sufficient accuracy as the distance at which the calculated wall temperature is very close to the interface temperature, e.g., where

$$\left(T - T_i\right) = 0.1\,°F \quad .$$

This length is then used in the second iteration in evaluating h_b. The temperature distribution is recalculated, and the evaporator length is determined again. The iteration is continued until the calculated value of h_b is constant, within prescribed limits, between iterations. The appropriate value of h_b and the correct temperature distribution have then been approximated.

b. Condensation Heat Transfer. The state of knowledge of condensation heat transfer is similar to that of boiling heat transfer. Agains, the difficulty encountered is that the available correlations for calculating the condensation heat transfer coefficient, h_c, contain gravitational acceleration coefficients and were developed for unwicked surfaces. Thus, if it is desirable to predict heat pipe performance, the only alternative is to again assume that the shape and motion of the liquid phase in a capillary structure are independent of gravitational acceleration and to utilize the available correlations developed for the 1-g environment to estimate the heat transfer coefficient. The designer is handicapped even further here than in the boiling situation because no known data exists for condensation onto wick type structures. As a first approximation, the following relation from Reference 13 for laminar condensation on horizontal tubes may be utilized to estimate the condensation coefficient:

$$h_c = 0.725 \left[\frac{k_\ell^3 \, \rho_\ell^2 \, g \, \lambda}{D_i \, \mu_\ell \left(\Delta T_{sat}\right)} \right]^{\frac{1}{4}} \tag{36}$$

50

where

h_c — average condensation heat transfer coefficient, $Btu/hr-ft^2-°R$

k_ℓ — thermal conductivity of condensate film, $Btu/hr-ft-°R$

ρ_ℓ — density of liquid in wick, lbm/ft^3

g — acceleration of gravity, ft/hr^2

λ — latent heat of condensation, Btu/lbm

D_i — inside diameter of tube, ft

μ_ℓ — dynamic viscosity of liquid in wick, $lbm/hr-ft$

ΔT_{sat} — difference between saturated vapor and condensing surface temperature, °R.

In applying this equation, the acceleration of gravity, g, should be taken as 1 - g to obtain film coefficients of the same magnitude as on Earth. The difference ΔT_{sat} between the saturated vapor and the condensing surface is not known a priori, but is of necessity relatively small because coefficients of condensation heat transfer are generally very large. An iterative procedure may be used to determine an appropriate value of ΔT_{sat}.

Obviously, the procedure described here for estimating condensation heat transfer coefficients is very crude, and should be considered for only the most preliminary heat pipe performance calculations. As improved correlations become available for reduced gravity condensation on wicked surfaces, the crude procedure described here should be replaced.

2. Sample Calculation of Temperature Distribution Near Ends of Heat Pipe Between Source and Sink. To illustrate the computational procedure and the rapid dissipation of heat flow near the ends of the heat pipe, a hypothetical problem was analyzed for the configuration shown in Figure 20. The inputs utilized in the calculations are listed in Table 2.

TABLE 2. INPUTS UTILIZED IN SAMPLE CALCULATION OF TEMPERATURE DISTRIBUTION NEAR ENDS OF HEAT PIPE BETWEEN SOURCE AND SINK

Item	Data

Enclosure

Item	Data
Material	Aluminum
Outside diameter	2 in.
Wall thickness	0.05 in.
Length	3 ft
Thermal conductivity	120 Btu/hr-ft-°R

Capillary Structure

Item	Data
Material	Aluminum wire mesh
Porosity	0.8
Mean fiber diameter	0.0002 in.
Wick thickness	0.32 in.

Working Fluid

Item	Data
Fluid	Water
Surface tension	0.0045 lbf/ft
Contact angle	0 deg (perfect wetting)
Prescribed saturation temperature	150°F

Heat Load

Item	Data
Heat load	500 Btu/hr

Considering the inputs of Table 2, the average boiling and condensation heat transfer coefficients were estimated to be 2 282 and 1 950 Btu/hr-ft^2-°R, respectively. The boiling heat transfer coefficient was based on a length of boiling surface of 1 inch, which was confirmed by temperature calculations to be approximately correct. The condensation heat transfer coefficient was based on an assumed average temperature difference, ΔT_{sat}, of 10°R.

The results of the sample problem calculations are shown in Figure 21. Calculated heat pipe wall temperature is plotted as a function of axial distance from the hot and cold ends, for a prescribed liquid interface temperature of 150°F. As shown by Figure 21 almost all of the heat flow is absorbed by the working fluid within a distance of 1 inch from the hot end of the pipe. This is evidenced by the rapid decline of wall temperature to essentially the liquid interface temperature. Likewise, significant axial temperature variation at the cold end is limited to less than 1 inch of length. It is noted that the temperature drop between source and sink is approximately 73°F, which is extremely large for a heat pipe. The large variation is confined almost entirely to segments near the end attachment points. This large difference is attributed to the large resistance of the pipe wall to axial conduction at the attachment rings, caused by the small cross-sectional area of the pipe wall. The large temperature difference could be reduced appreciably by increasing the pipe diameter. Perhaps a more effective method would consist of modifying the attachment hardware such that the heat is added and extracted from the heat pipe radially over a relatively large surface area. In the latter case the only resistance to heat flow into the fluid would be the lateral resistance of the thin pipe wall. This should eliminate essentially all temperature drop between source and sink.

The radial temperature distribution in the end plates to which the heat pipe is attached may be calculated using the procedures defined by Reference 11.

D. Incorporation of Heat Pipe Concept into Spacecraft Radiator Design

Utilization of the heat pipe concept has been considered (Refs. 6, 14, 15, and 16) as a means of improving space radiator performance. Since the heat pipe is essentially an isothermal device, it may be used to eliminate the usual temperature differential between the tube and
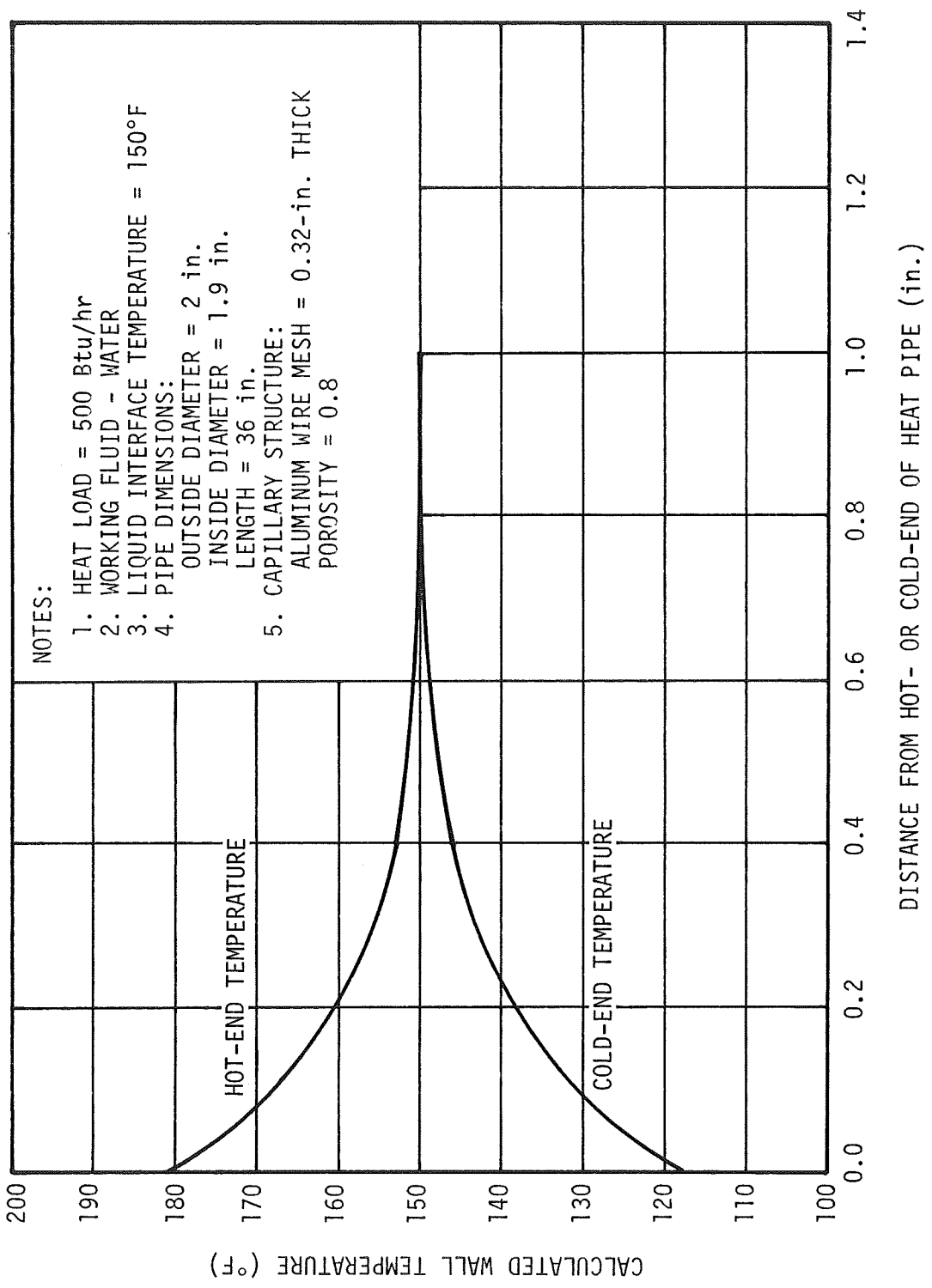
FIGURE 21. SAMPLE CALCULATION OF TEMPERATURE DISTRIBUTION NEAR ENDS OF HEAT PIPE BETWEEN SOURCE AND SINK

NOTES:

1. HEAT LOAD = 500 Btu/hr
2. WORKING FLUID - WATER
3. LIQUID INTERFACE TEMPERATURE = 150°F
4. PIPE DIMENSIONS:
   OUTSIDE DIAMETER = 2 in.
   INSIDE DIAMETER = 1.9 in.
   LENGTH = 36 in.
5. CAPILLARY STRUCTURE:
   ALUMINUM WIRE MESH = 0.32-in. THICK
   POROSITY = 0.8

54

solid fin of a conventional radiator. Because the radiator will be radiating at a higher average temperature, the required surface area will be reduced. All of the investigations reported to date have been analytical, and have been directed toward high power, nuclear space power supply systems. A review of these investigations is presented in Appendix A.

These investigations have predicted substantial weight savings by radiators incorporating heat pipes and vapor chambers over the conventional central tube and fin design. However, a weight savings may not be realizable with manned orbital vehicles such as the Saturn V Workshop, because the operating temperature is sufficiently low to permit integration of the conventional radiator into the spacecraft skin, thus using the skin structure as the radiator fin material. Radiator tubes are attached directly underneath the spacecraft skin. Hence, no weight penalty is attributed to the radiator fin, and a very light radiator results. Utilization of the heat pipe concept in radiator design usually requires a double-wall structure containing a working fluid between tubes. Whether a weight savings could be achieved using a heat pipe radiator would depend on whether the weight reduction obtained by the decrease in required surface area would be greater than the weight added by the additional wall thickness and working fluid.

Two design concepts have been considered in the investigations to date. In the first, proposed by Haller, et al of NASA (Refs. 14, 15, and 16), the solid fin of the conventional radiator is replaced by what is termed a vapor chamber-fin. A representative geometry for a vapor chamber-fin radiator is shown in Figure 22. The operation of the vapor chamber-fin is similar to that of the conventional heat pipe. A working fluid in the chamber is boiled off the tube surface and condensed on the fin surface of the chamber to produce a fin of constant temperature. Condensate is then returned to the boiling surface by capillary action in the wick. Reference 14 presents a detailed description of complete design procedures which may be utilized to design a radiator of this type. Included are a heat transfer analysis of the vapor chamber and tube block, capillary fluid requirements, meteoroid protection criteria, pressure drop analysis, weight calculation and thermal degradation due to meteoroid puncture of some of the vapor chambers. The description of Reference 14 is considered sufficiently complete that further discussion here of design equations and procedures is unnecessary. These procedures could easily be adapted to programmed solution by a digital computer such that rapid parametric analysis could be performed.
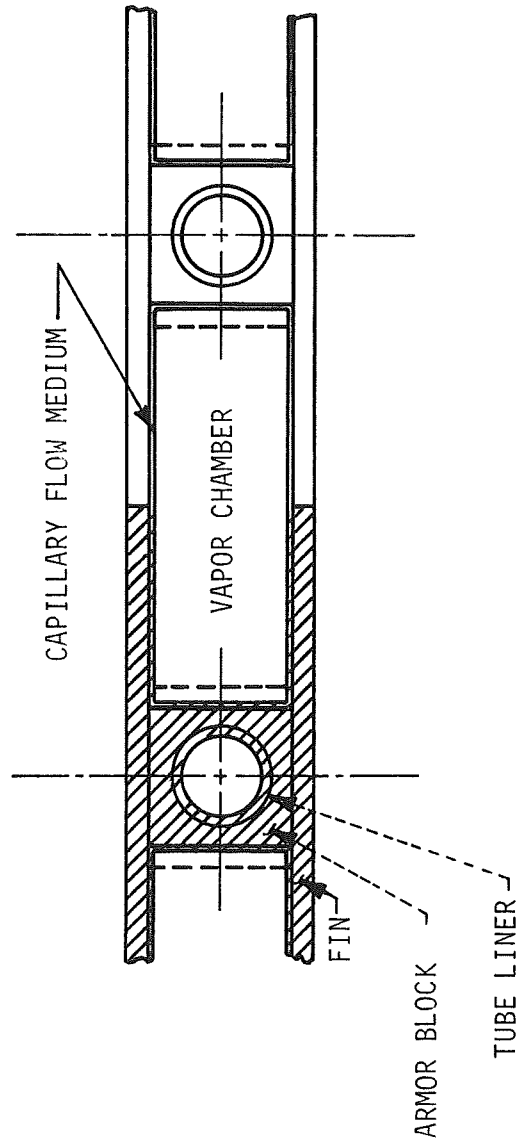
FIGURE 22. VAPOR CHAMBER-FIN RADIATOR (From Ref. 14)

The vapor chamber-fin approach has one heat transfer limit that adversely affects its performance. The fluid-carrying tubes are always separated from the vapor chamber by a meteoroid barrier thickness which creates a significant temperature drop between the fluid in the tube and the vapor in the fin. Since heat rejection is a fourth-power function of the vapor chamber wall temperature, any temperature differential between fluid and radiating surface lowers effectiveness and creates a heavier system.

Reference 6 introduced a second heat pipe radiator concept that allegedly overcomes the dilemma of having to provide sufficient meteoroid protection without sacrificing heat transfer capability. This second concept, illustrated by Figure 23, consists of inserting the ends of many small heat pipes into the fluid-carrying tubes such that the heat pipes are in direct contact with the primary fluid. The heat pipes can thus be supplied heat directly from a fluid source which is protected from meteoroids without suffering the temperature drop associated with the meteoroid barrier of the vapor chamber-fin concept. The heat pipes operate in parallel, functionally independent from one another. Because many independent heat pipes are involved, they can be designed for a minimum weight for a specified probability that a certain fraction will remain unpunctured throughout the mission. The effect of the puncture of a single heat pipe is only that it will cool and not contribute as effectively as a heat transfer member. Since a large number are involved, and redundancy can be incorporated, the loss of a considerable number can be tolerated.

Reference 6 contains design procedures which apply to this type of heat pipe radiator.

It may be concluded from this discussion of heat pipe radiators that introducing the heat pipe concept into radiator design appears to be technically feasible, and almost certainly will result in a reduction in required surface area.

It seems doubtful that a heat pipe radiator having even a smaller surface area could be lighter than a conventional tube and fin radiator which utilizes the vehicle skin as the fin. However, utilizing a heat pipe radiator could be advantageous in a situation where the radiator must be deployable. To compare decisively the weight of a heat pipe radiator with a conventional fin and tube radiator for any situation would require a detailed system optimization study of each design based on the constraints of the situation in question, which is beyond the scope of this work.

HEAT
PIPES

DUCT

LIQUID
IN

LIQUID
OUT
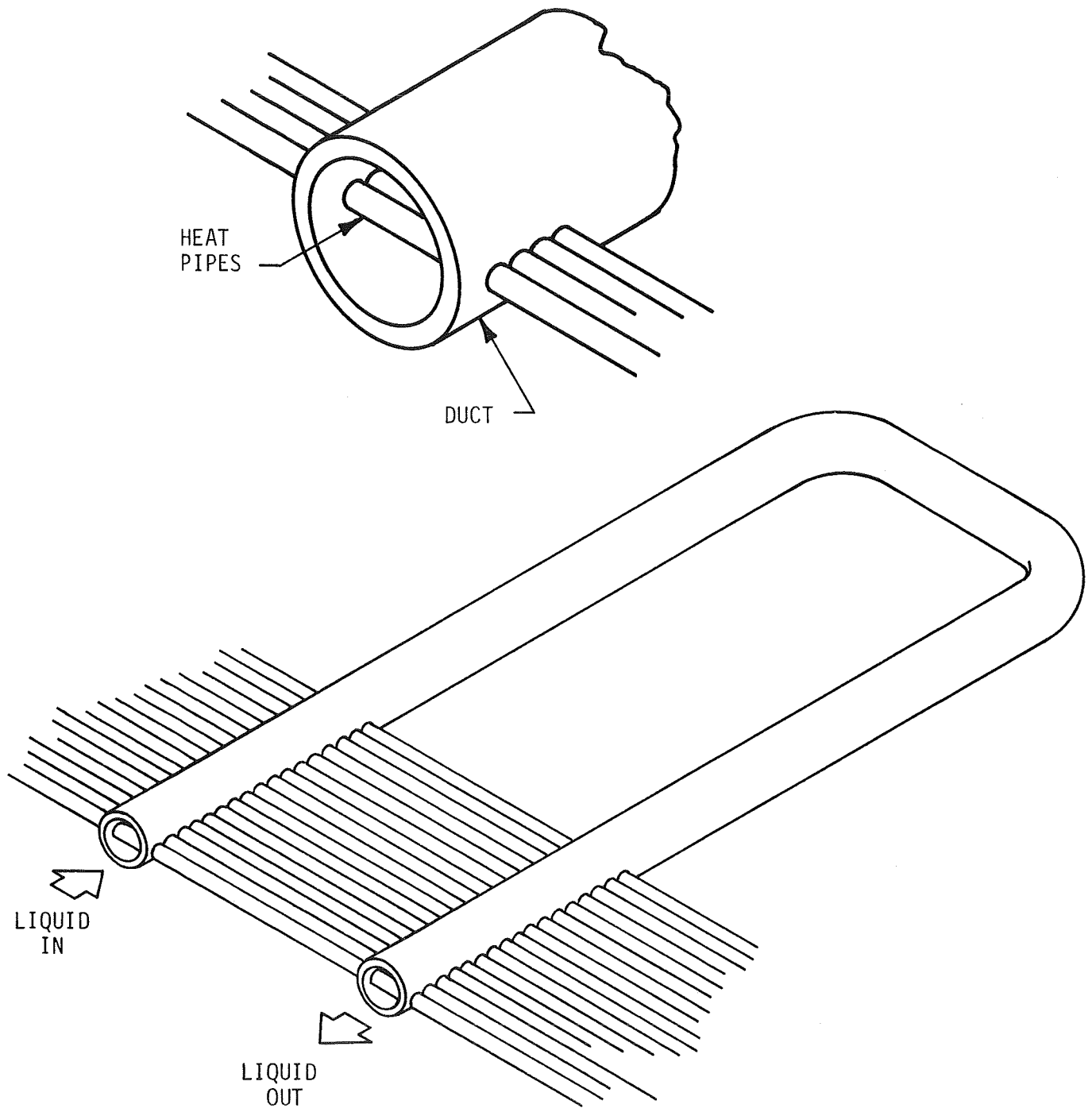
FIGURE 23.   HEAT PIPE RADIATOR CONCEPT (from Ref. 6)

58

SECTION IV. CONCLUSIONS

The heat pipe is obviously a practical, highly effective device for efficiently transporting large quantities of heat which will no doubt find many future applications in both aerospace and commercial industries. The engineering analysis of heat pipe systems involves three kinds of problems. Given a specification of a heat pipe and a prescription of its thermal coupling with the external environment:

- What are the actual distributions of temperature during operation?

- What is the maximum power limit for the working range of heat fluxes?

- What transient operating conditions are required to bring the heat pipe to the operating conditions?

In the prediction of temperature distributions during operation, perhaps the most serious lack of knowledge is in the area of estimating evaporation and condensation heat transfer coefficients for wicked structures in reduced gravity acceleration fields. A large amount of experimental work is needed in this area.

In establishing maximum power limits of heat pipes, most of the analysis to date has assumed constant heat addition along the evaporator length, and constant heat removal along the condenser length. Methods need to be developed for predicting maximum power limits considering other forms of heat addition and removal.

Little work has been devoted to analyzing the transient start-up phase of heat pipe operation. Experiments described by Reference 5 showed that start-up of a frozen heat pipe is critical, and that failure can occur even at low power input levels. Additional analysis and experimentation of the transient phase is needed.

This investigation has shown that present knowledge of the engineering physics of the heat pipe process is sufficient to permit realistic prediction of the general feasibility of a prospective new application, although available performance prediction techniques need to be proven by correlation of actual flight experiments before they may be applied with confidence to optimize specific designs.

60

APPENDIX A. LITERATURE SURVEY OF
HEAT PIPE TECHNOLOGY

The feasibility of utilizing the phase change characteristics of a working fluid to transfer large quantitites of heat was investigated as early as 1960 (Ref. 17). In these tests a water-saturated porous felt pad was attached to the lower side of a heated steel plate in a simulation of electronic cooling. Plate temperature, felt temperature and residual weight were recorded versus time. It was noted that there was a very small temperature difference between the heated plate and the felt pad, and that the evaporation process was very effective in maintaining the heated plate at the saturation temperature of the working fluid.

A. Introduction of Heat Pipe Concept

The "heat pipe" concept considered in this investigation was introduced by Grover, Cotter, and Erickson (Ref. 1). The device consisted of a closed outer shell, a porous wick and a working fluid as shown in Figure 1.

In the initial qualitative experiment water was used as the working fluid in a pyrex tube. The capillary structure, or wick, consisted of a porous Alundum tube, 2.5 cm outside diameter, 1.9 cm inside diameter, and 30 cm long. The pyrex tube fit tightly around the inserted capillary structure. Enough water was added to saturate the wick with a small excess. The pressure in the tube was lowered by pumping at room temperature until the resulting boiling swept out all but water vapor from the central gas space. The tube was then sealed. An evacuated blank of identical structure containing no water was also prepared. The heat pipe and the blank were arranged side by side, and the top 10 cm of the tubes were exposed to an infrared lamp. Within a few minutes the bottom of the heat pipe became and remained uncomfortably hot to the touch, whereas the bottom of the blank stayed nearly at room temperature.

Following the initial qualifying experiment, tests were conducted on a 347 stainless steel tube, employing liquid sodium as the working fluid. The wick, made of 100 mesh 304 stainless steel screen with 0.13-mm-diameter wires, was formed in a spiral of five layers and fitted closely against the inner wall of the tube to leave an inside diameter of 1.3 cm. The heat pipe was placed in a vacuum chamber

and about 13 cm at one end was heated by electron bombardment from a concentric spiral filament. Heat was rejected along the pipe length by radiation, with vapor condensation along the entire heated section. The heated end was elevated 4 cm above the unheated end. At a power input of 1 kW, the heat pipe operated at about 1 100°K. Steady state temperatures were measured along the heat pipe at a number of input power levels. These temperature measurements are reproduced here in Figure A-1. The temperature plateaus indicate the length of pipe in which refluxing (return of the liquid condensate by capillary action) occurred. The regions of rapidly decreasing temperature were attributed to the presence of hydrogen gas, a well known impurity in sodium metal, toward the cooler end of the pipe. The hydrogen is swept toward the unheated end of the pipe by the flow of sodium vapor. In the hydrogen region, the heat flow is accomplished by ordinary thermal conduction, mainly by the container wall and the saturated wick. Although measurement methods were not precise enough to detect the temperature gradients, they did not exceed 0.05°K/cm.

B.   Development of Heat Pipe Theory

Following the introduction of the heat pipe concept and initial qualitative experiments, the basic theory of heat pipe operation was set forth in analytical form by Cotter (Ref. 2). His discussion was limited to right circular cylinders of large length-to-diameter ratio. Only the highlights of Cotter's investigation are presented here.

The interface between the liquid in the capillary structure (wick) and the adjacent vapor must assume a local radius of curvature, r, such that the surface tension, σ, supports the difference in pressure between the liquid and the vapor. This pressure difference is expressed as

$$P_v - P_\ell = \frac{2\sigma}{r} \quad .$$

(A-1)

In a capillary structure of minimum pore radius, r_c, containing a liquid for which the contact angle is θ, the smallest radius of curvature that the meniscus can achieve is $r_c \sec \theta$. The liquid-vapor interface under some circumstances may be at the surface of the capillary structure, or even outside it. Thus, the maximum radius of curvature may be at least as large as the radius of the vapor space.
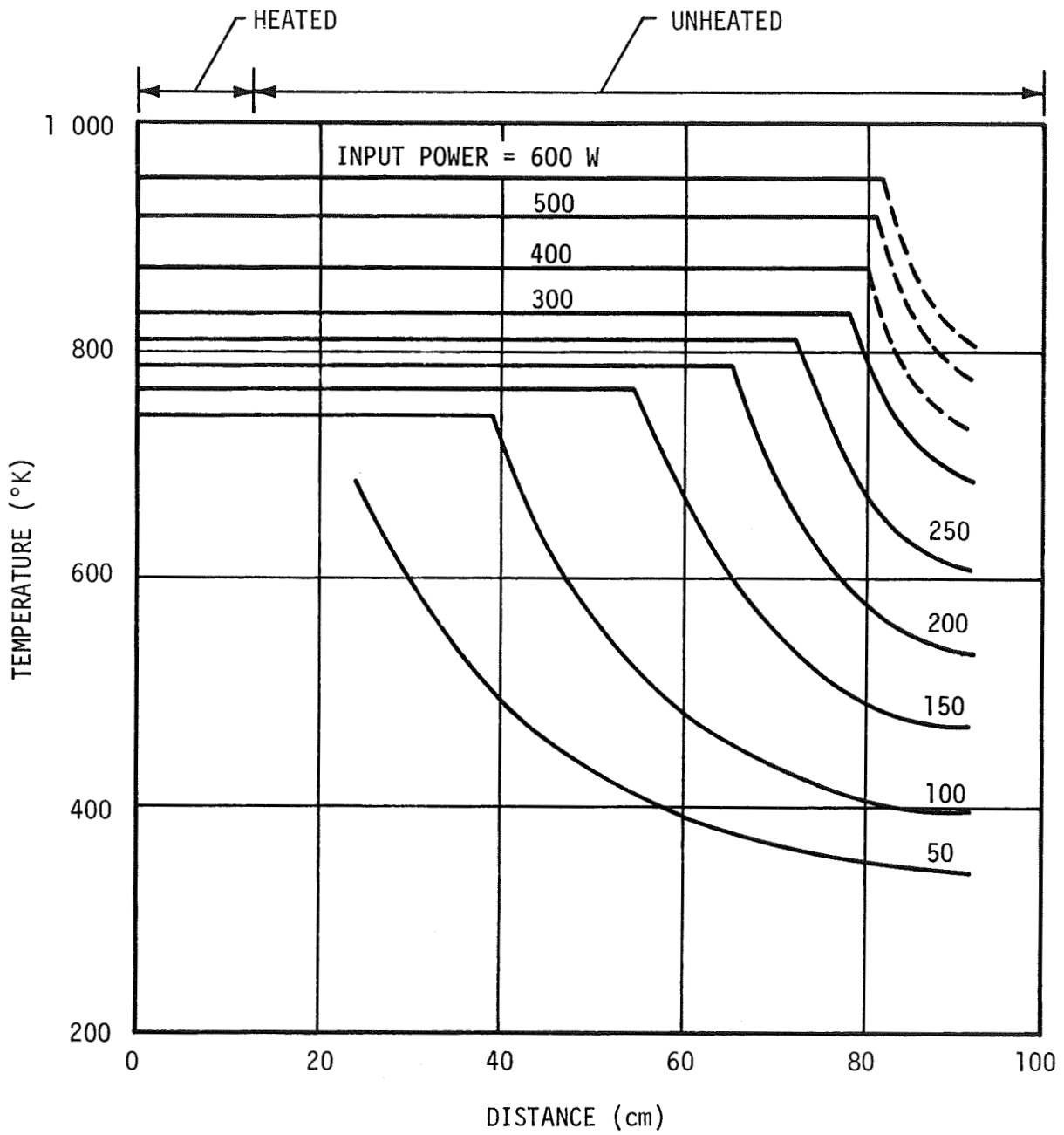
FIGURE A-1. TEMPERATURE PROFILES OF A 90-CENTIMETER HEAT PIPE
            (FROM REF. 1)

63

In a gravity field, the maximum vertical height of capillary rise, $L \sin \phi$ (see Figure 1), is

$$L \sin \phi = \frac{2\sigma \cos \theta}{\rho_\ell \left(\dfrac{g}{g_c}\right) r_c} \quad . \tag{A-2}$$

Thus, in a gravity field, the length of the heat pipe must not exceed L for proper operation. It is seen that as $\phi \to 0$, gravitational effects approach zero, and the maximum heat pipe length becomes unlimited by Equation A-2. This relationship is often used to simulate heat pipe operation in the 0-g environment.

Cotter also derived equations for the distribution of energy flow, material flow, temperature and pressure within a heat pipe during steady state operation. Basic working relations were obtained from the general equations of conservation of mass, momentum and energy by taking averages over the radial cross section of the pipe and making simplifying assumptions.

The derived relation for axial pressure gradient of the liquid in the capillary structure was reported as

$$\frac{dp_\ell}{dz} = \rho_\ell \frac{g}{g_c} \sin \phi - \frac{b \, \mu_\ell \, \dot{m}_\ell(z)}{\pi \left(r_w{}^2 - r_v{}^2\right) \rho_\ell \, \epsilon \, r_c{}^2 \, g_c} \quad . \tag{A-3}$$

Equation (A-3) is similar to Darcy's law for laminar flow through porous media.

The vapor flow in the evaporation and condenser of a heat pipe is dynamically identical to pipe flow with injection or suction through a porous wall. It is assumed that the flow is laminar and incompressible, with uniform injection or suction. Several regimes as distinguished, depending on the magnitude of a Reynolds number, R_r, based on the radial flow velocity at the channel wall, v_r, the channel radius, r_v, the vapor density, ρ_v, and dynamic viscosity, μ_v. Thus,

$$R_r = - \frac{\rho_v \, r_v \, V_r}{\mu_v} \tag{A-4}$$

where R_r is positive for evaporation and negative for condensation. For $|R_r| << 1$, viscous effects dominate and the axial velocity profile is close to the usual parabolic shape for Poiseville flow. The differential equation reported for the axial pressure gradient in this regime ($R_r << 1$) is

$$\frac{dp_v}{dz} = \frac{-8 \, \mu_v \, \dot{m}_v}{\pi \, \rho_v \, r_v^{\,4} \, g_c} \left(1 + \frac{3}{4} R_r - \frac{11}{27} R_r^{\,2} + \cdots \right) . \qquad (A-5)$$

This expression is derived on the assumption that R_r is constant, independent of z.

When $|R_r|$ is large the evaporation and condensation cases become qualitatively different. For large evaporation rates, $R_r >> 1$. The total pressure decreases in the direction of flow. With large condensation rates on the other hand, the flow is of the boundary layer type. The axial velocity is constant across most of the channel, with the transition to zero velocity occurring in a thin layer at the wall. The pressure increases in the direction of fluid motion because of partial dynamic recovery in the decelerating flow. In this regime only the limiting behavior ($|R_r| \rightarrow \infty$) are reported on. In either limit (evaporation or condensation) the pressure gradient is reported as

$$\frac{dp_v}{dz} = - \frac{s \, \dot{m}_v}{4 \, \rho_v \, r_v^{\,4} \, g_c} \frac{d \, \dot{m}_v}{dz} \qquad (A-6)$$

where the difference in flows enters only in the numerical coefficient s: for evaporation, s = 1; for condensation, $s = 4/\pi^2$. As before, this equation is strictly correct only for constant R_r.

The final expression describing the flow dynamics determines the relationships between the vapor and liquid mass flows and their pressures. The interface meniscus assumes a radius of curvature satisfying Equation A-1 and is a function of the axial location z. The two mass flows are coupled with the liquid temperature at the interface, which determines the vapor pressure of the liquid, p_ℓ'. The local condensation rate $d \, \dot{m}_\ell/dz$ is given by the gas kinetic formula

$$\frac{d \, \dot{m}_\ell}{dz} = - \frac{d \, \dot{m}_v}{dz} = \frac{\alpha \, r_v \left(p_v - p_\ell' \right)}{\left(\overline{R}T/2 \, \pi \, M \right)^{\frac{1}{2}}} . \qquad (A-7)$$

The numerical factor $\alpha \simeq 1$ reportedly includes both the probability of condensation of an impinging vapor molecule, and the "roughness" of the meniscus interface formed on the capillary structure. This equation applies for evaporation, but not for boiling evaporation, i.e., formation of bubbles in the capillary structure.

Considering the transport of energy, Cotter derived the somewhat obvious conclusion that the axial transport of energy is essentially entirely accomplished by the vapor convection of latent heat of vaporization. Thus,

$$Q(z) = \lambda \, \dot{m}_v(z) \quad . \tag{A-8}$$

The differential equations described above for steady state heat pipe operation were solved by Cotter for the case of constant heat addition along the evaporator and constant heat removal along the condenser. The reported equation for total pressure drop in the vapor is

$$P_{v_L} - P_{v_o} = \begin{cases} \dfrac{-4 \, \mu_v \, L \, Q_e}{\pi \, \rho_v \, r_v^{\,4} \, \lambda \, g_c} & ; \quad R_r \ll 1 \\[4mm] \dfrac{-\left(1 - 4/\pi^2\right) Q_e^{\,2}}{8 \, \rho_v \, r_v^{\,4} \, \lambda^2 \, g_c} & ; \quad R_r \gg 1 \quad . \end{cases} \tag{A-9}$$

The decrease in vapor pressure of the liquid in the direction of vapor flow is given as

$$P_{\ell_L}{}' - P_{\ell_o}{}' = P_{v_L} - P_{v_o} - \frac{L \, Q_e \left(\overline{R} T_o / 2\pi M\right)}{L_e \, (L - L_e) \, \lambda \, \alpha \, r_v} \quad . \tag{A-10}$$

The equation for liquid pressure drop, found by integrating Equation A-3, is

$$P_{\ell_L} - P_{\ell_o} = \rho_\ell \left(\frac{g}{g_c}\right) \sin \phi + \frac{b \, \mu_\ell \, Q_e L}{2\pi \left(r_w^{\,2} - r_v^{\,2}\right) \rho_\ell \, \epsilon \, r_c^{\,2} \, \lambda \, g_c} \quad . \tag{A-11}$$

While the thermal conductance of a heat pipe is very large, there are limitations on the magnitudes of both the total and local energy fluxes. The total axial heat transport may increase only if the pressure differential generated by capillary action can sustain the required circulation of fluid. The maximum pressure difference between vapor and adjacent liquid that can be supported by surface tension in the wick is

$$\frac{2\,\sigma\,\cos\,\theta}{r_c} \quad .$$

It is therefore necessary that

$$p_v - p_\ell \leq \frac{2\,\sigma\,\cos\,\theta}{r_c} \tag{A-12}$$

at all axial locations ($0 \leq z \leq L$).

If the heat pipe has been prepared with a fully saturated wick, the vapor-liqiud interface meniscus will have large radius of curvature of the terminal end of the condenser, and therefore, from Equation A-1, $p_{v_L} \simeq p_{\ell_L}$. In general, the largest pressure difference will occur at the beginning of the evaporator section, $z = 0$. Thus, if Equation A-12 is satisfied at $Z = 0$, it will be satisfied for all z. To insure adequate circulation, then

$$p_{v_o} - p_{\ell_o} \leq \frac{2\,\sigma\,\cos\,\theta}{r_c} \quad . \tag{A-13}$$

Thus, assuming that $p_{v_L} \simeq p_{\ell_L}$, Equations A-9, A-11, and A-13 may be combined to yield

$$\frac{2\,\sigma\,\cos\,\theta}{r_c} \geq \frac{b\,\mu_\ell\,Q_{max}\,L}{2\,\pi\left(r_w^2 - r_v^2\right)\rho_\ell\,\epsilon\,r_c^2\,\lambda\,g_c} + \rho_\ell\,\frac{g}{g_c}\,L\,\sin\,\phi$$

$$+ \left.\begin{array}{l} \dfrac{4\,\mu_v\,L\,Q_{max}}{\pi\,\rho_v\,r_v^4\,\lambda\,g_c} \\[2mm] \\ \dfrac{\left(1 - 4/\pi^2\right)Q_{max}^2}{8\,\rho_v\,r_v^4\,\lambda\,g_c} \end{array}\right\} \begin{array}{l} R_r \ll 1 \\[4mm] \\ R_r \gg 1 \end{array} \quad . \tag{A-14}$$

Equation A-14 imposes an upper limit on the rate of heat addition to the evaporator section, beyond which the rate of evaporation will exceed the flow rate of the returning condensate, thus leading to termination of effective heat pipe operation.

Cotter also derived an expression for the optimum choice of capillary pore radius, r_c, for the case of uniform heat addition and removal. This value of r_c permits the maximum rate of heat transfer, Q_e, to the evaporator section for given values of r_w, r_v, L, ϵ, λ, θ, μ_ℓ and b. According to Cotter, optimum value of r_c results when the viscous contribution to Δp_ℓ is one-half the magnitude of the capillary pressure term, $\dfrac{2 \sigma \cos \theta}{r_c}$. For uniform heat addition and removal,

$$r_{c_{opt}} = \frac{b \mu_\ell Q_e L}{4 \pi \left(r_w^2 - r_v^2\right) \rho_\ell \lambda \sigma \cos \theta g_c} \quad . \tag{A-16}$$

If the hydrostatic contribution to Δp_ℓ is absent, and if the ratio r_v/r_w is not constrained, Cotter shows that the optimum value of r_v/r_w is 2/3.

C. Application of Heat Pipes to Space Thermionic Power Supplies

A major problem with nuclear space power supplies is that the waste heat can only be dissipated through radiation. The heat pipe represents a device for moving this heat with a minimum temperature drop and with no external fluid pumping systems which tend to lower the system reliability and increase the weight. Reference 18 pointed out some possible applications of the heat pipe to space thermionic power supplies, as listed below:

- Cooling of the moderator by a heat pipe system

- Solution of radiator reliability and weight problems caused by meteorite puncture by use of heat pipes in parallel. Since the puncture of one of the heat pipes in parallel would only fractionally reduce the radiator effectiveness, a minimum of meteorite shielding is required.

- Possible removal of heat from the reactor at the emitter temperature. Each fuel rod would consist of a heat pipe

with the uranium containing fuel attached externally to the pipe. The pipe would extend through the reflector, and a thermionic converter would be located on the extended portion of the pipe. This arrangement allows the converter to be made of materials suitable to the converter without regard to their neutron absorption cross sections.

● Elimination of troublesome thermal gradients along emitters and collectors.

Reference 18 also presents calculated characteristics data for a heat pipe in which the capillary structure consists of channels cut into the inner surface and running axially the length of the tube. It was further assumed that fully developed laminar flow existed in both the liquid and vapor flow streams.

Reference 19 presented a conceptual design of a space power system employing out-of-pile thermionic diodes and using concentric heat pipes for both heating and cooling of these diodes. It was pointed out that the utilization of heat pipes in the reactor-thermionic provides several advantages. Since the heat pipe transfers large amounts of heat with very small temperature drop, it is possible to obtain a diode emitter surface with a temperature close to the temperature of the fuel clad while being located outside the core. Then, since the heat pipe is practically an isothermal heat transfer device, it may be possible to operate many thermionic diode emitters at the same temperature even though the power density generated throughout the reactor is not constant. This alleviates the amount of power tailoring that needs to be done in the reactor. Also, if the thermionic diodes are placed outside the reactor core, diode shorting caused by fuel swelling is eliminated. It then becomes possible to design diodes with smaller spacing between emitter and collector and reap higher values of power level and efficiency. Furthermore, the electrical insulation material can be removed from high radiation regions and thus reduce the damage by fast neutrons.

Laboratory data on the performance of heat pipes was examined to estimate reasonable performance levels for thermionic diodes, which were incorporated into a small, fast-spectrum nuclear reactor concept. Performance levels and system weights were estimated from first-order calculations.

Reference 20 describes a two-year program in which the practicality of joining thermionic modules was demonstrated. The two-year program culminated in the achievement of over 3 000 hours of test time for a module-heat pipe combination which maintained an average power output of 2. 0 W/cm^2 without degradation in performance.

D. Experimental Studies of Heat Pipe Capability

Following the introduction of the heat pipe concept and the initial qualitative experiments, several tests have been conducted to evaluate heat pipe performance under varying operating conditions.

The first heat pipe development program which was directed toward a specific application was conducted by Los Alamos Scientific Laboratory (Ref. 8). In this program a heat pipe was developed for the Applied Physics Laboratory of Johns Hopkins University which was to be used in a satellite to transfer heat isothermally from an externally mounted radioisotope to the electronic component section. The intended purpose of this system was to reduce the amplitude of thermal cycling of the components in orbit. The heat pipe, lined its full length with a stainless steel wick structure, was constructed of stainless steel, and used water as the working fluid. Heat from the isotope capsule was to be transferred to the pipe through an aluminum block assembly. The tube was 29.625 inches long and 0. 75-inch outside diameter with a 0.016-inch wall. The wick structure was formed by rolling 100 mesh screen into a hollow cylinder of two layers, which was inserted into the tube. A steel ball was then pushed through the hollow screen cylinder to press it against the wall. To assure continued contact of the wick with the wall under operating conditions, a tungsten helical spring was pulled into the full length of the wick structure under tension and then released to provide additional radial pressure.

The heat pipe was tested under simulated space conditions by operating it in a vacuum chamber with the pipe nearly horizontal to eliminate gravity effects. The heat input end was slightly elevated to determine if proper wicking action was occurring. The heat pipe was mounted in a fin assembly similar to the satellite strut, which was attached to a water-cooled heat sink to simulate heat absorption by the electronic component section. An electric resistance heater was used to mock-up the isotope heating. Temperatures were measured along the outer surface of the heat pipe, and the temperature rise and flow

rate of the cooling water were measured to determine the rate of heat transfer from the condenser section of the heat pipe. Power input was calculated from input voltage and current measurements. A vacuum of 10^{-6} mm Hg was maintained during the tests. Results of this test indicated that the heat pipe was almost isothermal at 93°C over its entire length. With a heat input of 102.8 watts, 95 watts were transferred to the cooling water.

A separate test was made in air to determine the maximum vertical wicking height of the heat pipe in a gravity field. This was done by mounting the heat pipe and fin assembly on a pivot perpendicular to the heat pipe axis. By rotating the heat pipe assembly on the pivot, the vertical wicking height could be varied. Maximum vertical wicking height was determined by increasing the heat pipe angle during operation until a sharp temperature rise in the source block temperature was noted. This indicated that the wick in the heat input zone was drying out as the water evaporating from the wick could not be replaced by wicking action.

The maximum vertical wicking height for this particular wick structure was determined to be 8 inches. This indicates that the water was wetting the stainless wick structure adequately. In free space, the wicking height would theoretically be infinite. Sufficient liquid flow into the evaporator zone is then a function only of the dynamic flow resistance of the wick structure and the evaporation rate set by the heat input flux.

One model was built and operated continuously to determine if any buildup of noncondensable gases occurred due to the interaction of water and stainless steel. The heat pipe was mounted in a water-cooled strut assembly and operated in air with a heat input of 100 watts. The assembly was insulated with fiber glass to approximate the temperature conditions obtained in vacuum operation. The life test model was operated for over 3 000 hours. No change was noted in the temperature pattern, indicating that noncondensable gases had been formed to any appreciable extent.

An experiment was conducted by Johns Hopkins University (Ref. 9) to correlate heat transfer coefficients in the evaporator section of a heat pipe. Parameters measured included temperature distribution along the external wall of the tube and vapor temperature.

The wick boiling heat transfer coefficient is defined as

$$h_b = \frac{Q_e}{A_w \left(T_w - T_v\right)} \qquad \text{(A-17)}$$

71

and the liquid mass flow rate is

$$\dot{m}_\ell = Q_e/A_w \epsilon \lambda \quad . \tag{A-18}$$

The following correlation was obtained for the wick boiling heat transfer coefficient.

$$h_b = 0.0051 \ c_p \ \dot{m}_\ell \ P_r^{-0.6} R_e^{-1.43} \left(\frac{\sigma \ P_e}{P_\ell^2} \ \frac{g}{g_c}\right)^{-0.2} \quad . \tag{A-19}$$

Several experiments were conducted by Kemme (Ref. 4) to determine the maximum heat transfer capability of heat pipes with fixed outside dimensions, subjected to variations in fluid used, temperature of operation and geometry of the wick and vapor passage.

The heat pipes were made from flat nickel sheets rolled into cylindrical tubes about 0.75-inch outside diameter by 12 inches long. Prior to rolling, a capillary structure was formed by cutting many rectangular channels along the complete length of each sheet. The width and depth of these channels were varied for different sheets. After each heat pipe was tested with open capillary channels, a layer of fine mesh screen was added to cover the channels and separate them from the vapor passage. Ten heat pipe systems were chosen for tests.

Use of the screen liner over the grooves increased the maximum heating rate considerably. This increase was attributed to increased capillary driving force, and hence increased liquid return rate, when open channels are covered with screen.

With sodium as the working fluid, it was found that increased channel size permits greater heat transfer rates with open channels. However, the results indicated that this may not be the case during startup and at low operating temperatures.

Comparing potassium and sodium working fluids, sodium appeared to be superior at temperatures above 500°C, although potassium may be advantageous whenever vapor pressure drop tends to control heat transfer (low temperatures, small vapor passage).

Because potassium has relatively poor properties for heat pipe operation in the temperature range investigated by Kemme, it was used as the working fluid in wick variation studies. These tests consisted of maximum heat transfer measurements of heat pipes containing loose-fitting versus tight-fitting screens covering the longitudinal channels.

Increased maximum heat transfer rates, obtained with the loose fitting screen, were attributed to reduced pressure drop of the returning liquid, resulting from the additional flow path between the screen and the wall.

It was concluded from Kemme's experiments that heat transfer characteristics of heat pipes with fixed outside dimensions can be changed significantly by variations in wick structure. Kemme also confirmed that heat transfer limits can be predicted with some confidence for the type systems investigated using existing heat pipe equations.

Reference 10 reports experimental results of two heat pipes, differing primarily in the lengths of their condenser sections, which were built and tested to determine their limiting heat transfer rates. Heat Pipe A had a heater section 3.5 inches long separated from a 4-inch long condenser section by an 8.5-inch long adiabatic section. Heat Pipe B was different in that the heater section was 4 inches long and the condenser section was 13 inches long. The capillary structure consisted of monel beads held in place by a stainless steel retaining screen. The heat pipe diameter was not reported.

Results were presented which showed the maximum power limit of the heat pipes versus angle of inclination from the horizontal. Also shown were curves of maximum power limit as calculated by an Equation derived by Reference 10. Good agreement between experimental and calculated values was demonstrated. Wick temperatures versus axial distance were measured and recorded.

Reference 5 reported the results of a number of heat pipe experiments using various wick structures. Also included in this report were a development of heat pipe design equations and a discussion of various heat pipe fluids.

Two heat pipe systems were designed, operated and evaluated using wicks of refrasil, stainless steel screen and sintered copper fiber. The first was a 16-inch long copper heat pipe (1.5-inch tube) with a

0.125-inch thick sintered copper fiber wick. The heated area of the pipe was 9.42 in^2 and the condenser area was 28.2 in^2. Water was the working fluid. The second heat pipe was a 2-foot-long stainless steel 0.75-inch tube in which wicks of refrasil and stainless steel screen were inserted. The heated area of the pipe was 14.1 in^2 and the condenser area was 14.1 in^2. Both water and ethyl alcohol were used as a working fluid in this pipe.

In general, the condenser was cooled with water from the building supply at about 68°F for both heat pipes. However, some experiments were made with refrigerated coolant to observe the heat pipe operation as the working fluid became frozen in the wick. The startup of an initially frozen heat pipe was also performed.

One of the 2-foot long stainless heat pipes containing four layers of 105 mesh stainless steel screen and 18-cc of water was set up as a long-term test of heat pipe performance. The pipe was in a horizontal position to simulate zero gravity. The power input was about 100 watts.

As the heating rate to the evaporator was increased during each of the tests, the mechanism which caused all but one of the heat pipes to fail was a limitation in the rate which the wick could pump the condensate to the evaporator. The one exception was the pipe with a refrasil wick. In this case, boiling occurred between the wick and the pipe wall pushing the wick away from the wall and resulting in a burnout of the pipe. This occurred even at low power levels of 40 watts (0.44 W/cm heat flux in the evaporator) and, therefore, the studies with the refrasil wick were discontinued. However, the failure of the refrasil wick revealed two important points.

- The thermal conductivity of nonmetal wicks is too low for their use in heat pipes designed to transfer powers of hundreds of W/in^2 cross section.

- The wick structure should be bonded to the pipe wall to decrease the resistance to energy transfer.

The hydrodynamic limitation for the other heat pipes was evident from two facts:

- In experiments in which the condenser was lowered, a point was reached in which the wick dried out at the end furtherest from the condenser. The drying out was deduced from the temperature at this point becoming very high.

● The relative limits for water and ethyl alcohol were pre-
dictable from the hydrodynamic theory.

Conclusions drawn from the studies reported by Reference 9 are
summarized below:

● A sufficient understanding of heat pipe operation and fabri-
cation methods was obtained to allow design of a heat pipe
for spacecraft use.

● Liquids with large intermolecular forces are good heat pipe
working fluids because they have high surface tensions and
latent heats of vaporization. The liquid metals and polar
liquids such as water and ammonia are examples. Organic
liquids and cryogens are examples of liquids which are not
good heat pipe fluids.

● The power limitations of heat pipes studied here were due
to a capillary pumping limitation. This makes knowledge
of the wick pore size and specific permeability most
important for an accurate design of a heat pipe.

● The sintered copper fiber wick possessed a large capacity
for transferring power, but the wick was not bonded to the
heat pipe wall and the contact resistance to heat transfer
(between the wick material and pipe wall) resulted in a very
large overall temperature drop.

● The stainless steel wire wicks (105 mesh, 3.5 mil wire)
formed by rolling the wire on a mandril resulted in heat
pipes that were not reproducible in detail. Nevertheless,
the study produced enough information so that a reliable
heat pipe can be produced which will transfer as much as
500 watts in zero gravity. A long-term test of one such heat
pipe lasted 4 560 hours with only minor changes in its oper-
ating characteristics.

● Start-up of a frozen heat pipe, even at very low power levels,
may lead to a burnout.

A heat pipe experiment was performed by Reference 21 to extend
and verify the work of Grover at Los Alamos. The pipe itself was essen-
tially identical to the Grover pipe, that is, 0.75-inch outside diameter

by 36-inch-long stainless steel pipe with a 0.0625-inch wall. The pipe was sealed on both ends and contained a wire-screen wick and 40 grams of sodium. The testing method and apparatus were modified to provide a calorimeter at the cooled end and to allow for operation at different inclination angles, in order to exclude processes other than mass transfer of sodium liquid and vapor in a 24-inch insulated section. The experimental results essentially confirmed the Grover data and, in addition, showed that the pipe would operate at inclination angles five times greater than those used by Grover. An equivalent thermal conductivity of 1 900 W/cm-°C was measured, which is 540 times that of a solid copper cylinder. The wick pumped the liquid sodium back to the heated end against gravity at an inclination angle of 12 degrees.

A 2-year program reported by Reference 20 demonstrated the practicality of joining thermionic modules to heat pipes for efficient long-life operation. This program culminated in the achievement of over 3 000 hours of life test time for a heat pipe which maintained an average power output of 2.0 W/cm^2 without degradation in performance.

The results of this heat pipe development program indicated that a molybdenum heat pipe using lithium as the working fluid can be used as an efficient and reliable means for transferring large quantities of heat with very small temperature drop along the length of the pipe. It was recommended that additional work be performed in developing heat pipe processing techniques to provide purer lithium and cleaner internal heat pipe components, this being a necessity to ensure longer life at high operating temperatures. Additional wick studies were also recommended to provide capillary structures which provide maximum heat transfer efficiency.

E. Heat Pipe Experiment Under Zero-gravity Conditions

An orbital experiment was conducted (Ref. 22) to demonstrate that a heat pipe will operate, as predicted, in the absence of gravitational forces. The heat pipe was 12 inches long, 0.75-inch outside diameter and was constructed of a stainless steel tube lined its full length with a stainless steel wick structure. Water was used as the working fluid. It was operated in an Earth orbit and its performance was monitored by telemetry of several tracking stations during 14 revolutions. Heat was supplied to the heat pipe by a 10-watt electric heater. The satellite module in which the heat pipe was mounted was launched into orbit from Cape Kennedy by an Atlas-Agena launch vehicle.

The results of the orbital experiment indicated that the absence of gravitational forces does not affect the performance of a heat pipe. The start-up and equilibrium operations were similar to tests in a gravity field. There was not evidence to indicate that heat pipes using other fluids would not function in a similar manner.

F. Analytical Investigations of Space Radiators Utilizing the Heat Pipe Concept

In an effort to increase the radiating effectiveness, and thereby decrease weight, of solid fin waste-heat radiators of Rankine cycle space power systems, the vapor-chamber fin-tube concept was analyzed in References 14 and 15 for high- and low-power systems, respectively.

The vapor-chamber fin concept proposes to reduce radiator weight and area by providing for an essentially isothermal fin between tubes. In one approach, this can be accomplished by using a double-wall fin between tubes to form a hollow chamber which contains a fluid-soaked capillary medium along the inner surfaces, as shown by Figure 22.

Preliminary comparative analysis of an all-columbium radiator for a 500-kilowatt Rankine cycle electric power output system and of a beryllium fin and armor radiator for a 1-megawatt system were presented in Reference 14. These studies, which were based on the tube armor block configuration with a single value of tube nonpuncture probability of 0.995, indicated that the vapor-chamber fin-tube radiator concept can result in a sizable weight advantage, substantially smaller planform area, fewer number of tubes, and larger tube diameters than the central and double fin-tube radiators. Results of an analysis of the vapor chamber fin radiator for a low-power-level, low-temperature-level system (Ref. 15) indicated the vapor fin radiator had a lower weight than the solid conducting geometries for values of nonpuncture probability greater than 0.95. The vapor-chamber fin geometry always gave a substantially smaller planform area.

However, structural complexities and disadvantages in the use of vapor-chamber fin geometries were also revealed. In order to maintain a reasonable survival probability for the vapor-chamber fin without using large fin thicknesses, it was necessary to compartmentalize the vapor-chamber fins into many individual segments by the use of transverse and longitudinal bulkheads. Radiator weight can be minimized by the use of a large number of fin segments, which might involve problems in the

sealing of the individual segments. On the other hand, if a relatively small number of fin segments are used, the fin segment planform area might be large, so that stress and deflection problems might arise within the box-like structure of the vapor-chamber segments.

To obtain a more realistic evaluation of the theoretical weight and area gains achievable with the use of the vapor-chamber fin concept, a further analytical comparison was performed (Ref. 16) of radiators with block vapor-chamber fin-tube, central fin-tube, and double fin-tube geometries over a wider range of variables than considered in References 14 and 15.

This study showed that there is basically little difference in achievable specific planform area for the three geometries considered. However, minimum radiator specific weight was substantially different, with the vapor-chamber fin-tube radiator showing least weight in all cases. The magnitude of the weight differences will depend to a large extent on the specific input values chosen for the cycle and radiator components and on the comparison basis. Thus, an evaluation of the potential merit of a particular radiator fin-tube geometry should be based on a detailed weight and geometry analysis covering a wide range of input variables pertinent to the specific design application. At the same time, consideration should also be given to the possible complexities and unknowns involved in a particular geometric configuration which are not covered in the weight analysis. In the case of the vapor-chamber fin-tube radiator, such factors as the internal mechanics and thermodynamics of the capillary flow and possible structural complications involved in fin compartment sealing and buckling strength should be considered.

Another radiator concept employing heat pipes was investigated and reported on by Reference 6. As shown by Figure 23, the spaces between radiator tubes are occupied by many small, parallel heat pipes, the ends of which are inserted perpendicularly into the radiator tubes. Since the ends of the heat pipes are in direct contact with the radiator heat transport fluid, the temperature drop across the tube walls and meteoroid armor thickness, inherent in the vapor chamber concept, is eliminated. This should result in a more efficient radiating surface, thus reducing the required radiator area.

A representative heat pipe radiator was designed for a Rankine-cycle nuclear reactor power plant suitable for a manned Mars mission of 10 000 hours. The proposed radiator was estimated to reject 46 mW at 1 100 °K with a specific weight of 1. 322 lb/kWe.

78

G. Investigation of Heat Pipe Applicability to
Spacecraft Thermal Control Problems

One of the first investigations of applying the heat pipe concept to spacecraft thermal control problems was reported by Reference 11. This reference reviewed the theory of heat pipes, some possible applications, design computations and areas in which research and development are needed.

Three potential applications subjected to mathematical analysis by Reference 16 were:

- Maintenance of an evacuated cylinder at a uniform temperature by lining the inside surface with a saturated capillary structure

- Transfer of heat isothermally between parallel plates

- Improving temperature uniformity of an irradiated cylinder by wrapping heat pipes around the circumference at equal intervals.

Discussions were also included of wick design and multifluid operation.

APPENDIX B. INPUT DESCRIPTION AND FORTRAN LISTINGS OF COMPUTER PROGRAM FOR PARAMETRIC ANALYSIS OF MAXIMUM HEAT TRANSFER RATE OF HEAT PIPES

A FORTRAN computer program was developed to study the effect of variation in design parameters on maximum heat transfer rate of heat pipes. The maximum power that a heat pipe can maintain depends on the geometrical design parameters r_w, r_v, r_c, L, ϵ, b, and the working fluid properties μ_v, μ_ℓ, ρ_v, ρ_ℓ, σ, λ, and θ. These two groups were studied separately by holding one as a constant and varying the other. In terms of computer programming, this implies that there are two sets of input data for the program. For a given capillary structure the geometrical factors are fixed. The variation of working fluid properties corresponding to operating temperature was input to the computer program. Similarly, for a given fluid at given temperature, the variation in geometrical factor will be the input to the program. The detailed input guide and the FORTRAN listing are presented in this appendix.

DETAILED GUIDE FOR INPUT DATA

CASE I. Fixed Geometrical Factors

Card No. 1: This card specifies the given geometrical factor

Format	5E14.8	
Cols 2-15	SL	Length of heat pipe, ft
Cols 16-29	RV	Ratio of radius of vapor passage to inside radius of heat pipe
Cols 30-43	RW	Inside radius of heat pipe, ft
Cols 44-57	RC	Mean pore radius of capillary structure, ft
Cols 58-71	B	Dimensionless constant depending on the detailed geometry of the capillary structure.

Card No. 2: This card specifies geometrical factor and information on local acceleration of gravity

Format	5E14.8	
Cols 2-15	EPS	Fraction of wick volume occupied by liquid (or porosity)

Cols 16-29	PHI	Angle of inclination of heat pipe, deg
Cols 30-43	G	Local acceleration of gravity, ft/sec^2
Cols 44-57	GC	Dimensionless constant, 32.2 lbm-ft/lbf-sec^2

Card No. 3: This card gives information on working fluid properties corresponding to a working temperature

Format   5E14.8

Cols 2-15	TEMP	Working temperature, °F
Cols 16-29	ETAV	Dynamic viscosity of vapor, lbm/hr-ft
Cols 30-43	ETAL	Dynamic viscosity of liquid, lbm/hr-ft
Cols 44-57	RHOV	Density of vapor, lbm/ft^3
Cols 58-71	RHOL	Density of liquid, lbm/ft^3

Card No. 4: This card also specifies the working fluid properties at a working temperature

Format   5E14.8

Cols 2-15	GAM	Surface tension of working fluid in contact with capillary structure, lbf/ft
Cols 16-29	ZL	Latent heat of vaporization of liquid, Btu/lbm
Cols 30-43	TH	Contact angle between angle and capillary structure, deg

NOTE: For more information on working fluid properties
Card No. (2n + 1) Same as Card No. 3 n = 2, 3, 4, ...
Card No. (2n)   Same as Card No. 4 n = 3, 4, 5, ...

CASE II.   Fixed Working Fluid Properties

Card No. 1: Working fluid properties at a given temperature

Format   5E14.8

Cols 2-15	TEMP	Working temperature of heat pipe, °F
Cols 16-29	ETAV	Dynamic viscosity of vapor, lbm/hr-ft
Cols 30-43	ETAL	Dynamic viscosity of liquid, lbm/hr-ft

Cols 44-57 RHOV Density of vapor, lbm/ft^3

Cols 58-71 RHOL Density of liquid, lbm/ft^3

Card No. 2: This card also specifies the working fluid properties at a working temperature

Format   5E14.8

Cols 2-15 GAM Surface tension of working fluid in contact with capillary structure, lbf/ft

Cols 16-29 ZL Latent heat of vaporization of liquid, Btu/lbm

Cols 30-43 TH Contact angle between angle and capillary structure, deg

Card No. 3: This card specifies the geometrical factor

Format   5E14.8

Cols 2-15 SL Length of heat pipe, ft

Cols 16-29 RV Ratio of radius of vapor passage to inside radius of heat pipe

Cols 30-43 RW Inside radius of heat pipe, ft

Cols 44-57 RC Mean pore radius of capillary structure, ft

Cols 58-71 B Dimensionless constant depending on the detailed geometry of the capillary structure

Card No. 4: This card gives geometrical factor and information on local acceleration of gravity

Format   5E14.8

Cols 2-15 EPS Fraction of wick volume occupied by liquid (or porosity)

Cols 16-29 PHI Angle of inclination of heat pipe, deg

Cols 30-43 G Local acceleration of gravity, ft/sec^2

Cols 44-57 GC Dimensionless constant, 32.2 $lbm\text{-}ft/lbf\text{-}sec^2$

NOTE: For more information on geometrical factor
Card No. (2m + 1) Same as Card No. 3, m = 2, 3, 4, ...
Card No. (2m)   Same as Card No. 4, m = 3, 4, 5, ...

CASE I. GIVEN GEOMETRICAL FACTOR

```
200      FORMAT(39X,19HGEOMETRICAL FACTORS,/)
201      FORMAT(37X,24HWORKING FLUID PROPERTIES,/)
202      FORMAT(12H OUTPUT-----,/)
         WRITE(3,200)
         READ(2,100) SL,RV,RW,RC,B,EPS,PHI,G,GC
         RV=RV*RW
         WRITE(3,101) SL,RV,RW,RC,B
         WRITE(3,102) EPS,PHI,G,GC
         PHI=PHI/57.29578
100      FORMAT(5E14.8)
101      FORMAT(6H    SL=,F14.7,5H  RV=,F14.7,5H  RW=,F14.7,5H  RC=,F14.7,
        15H    B=,F14.7)
102      FORMAT(6H EPS=,F14.7,5H PHI=,F14.7,5H    G=,F14.7,5H  GC=,F14.7)
103      FORMAT(6H TEMP=,F14.7,5HETAV=,F14.7,5HETAL=,F14.7,5HRHOV=,F14.7,
        15HRHOL=,F14.7)
104      FORMAT(6H  GAM=,F14.7,5H    L=,E14.7,5H  TH=,F14.7)
105      FORMAT(6H TEMP=,F14.7,5H   NV=,E14.7,5H  B2=,F14.7,5H  B3=,F14.7,
        15H   XI=,F14.7)
106      FORMAT(6H   Q1=,E14.7,5H   Q2=,E14.7)
1        CONTINUE
         WRITE(3,201)
         READ(2,100) TEMP,ETAV,ETAL,RHOV,RHOL,GAM,ZL,TH
         WRITE(3,103) TEMP,ETAV,ETAL,RHOV,RHOL
         WRITE(3,104) GAM,ZL,TH
         TH=TH/57.29578
         PI=3.14159
         AV=PI*(RV    )**2
         AWV=PI*((RW   )**2-(RV    )**2)
         ZNV=(GAM*RHOV*ZL/ETAV)*417000000.
         XI=(G/GC)*RHOL*SL*RC*(SIN(PHI))/(2.*GAM*(COS(TH)))
         ZLAM=XI-1.
         C1=.34075
         C2=4.*(PI**2-4.)
         A1=AV/(RC*RC)
         A2=AV/AWV
         A3=B/EPS
         A4=RC/SL
         A5=A4**2
         A6=SL
         B1=ETAV*RHOL/(ETAL*RHOV)
         B2=1./B1
         B3=ZNV*    RC/(ETAV*ZL)
         B4=ZLAM
         B5=C2*COS(TH)
         B6=ETAV*ZL
         RAD=SQRT((B2*A2*A3)**2-(B3*B4*B5*A5))
         Q1=C1*A1*B6*A6*(-B2*A2*A3+RAD)
         Q2=C1*A1*B6*A6*(-B2*A2*A3-RAD)
         WRITE(3,202)
         WRITE(3,105) TEMP,ZNV,B2,B3,XI
         WRITE(3,106) Q1,Q2
         GO TO 1
         END
```

CASE II. GIVEN WORKING FLUID PROPERTIES

```
200      FORMAT(39X,19HGEOMETRICAL FACTORS,/)
201      FORMAT(37X,24HWORKING FLUID PROPERTIES,/)
202      FORMAT(12H OUTPUT-----,/)
         WRITE(3,201)
         READ(2,100) TEMP,ETAV,ETAL,RHOV,RHOL,GAM,ZL,TH
         WRITE(3,103) TEMP,ETAV,ETAL,RHOV,RHOL
         WRITE(3,104) GAM,ZL,TH
         TH=TH/57.29578
100      FORMAT(5E14.8)
101      FORMAT(6H    SL=,F14.7,5H   RV=,F14.7,5H   RW=,F14.7,5H   RC=,F14.7,
        15H    B=,F14.7)
102      FORMAT(6H   EPS=,F14.7,5H PHI=,F14.7,5H    G=,F14.7,5H   GC=,F14.7)
103      FORMAT(6H  TEMP=,F14.7,5HETAV=,F14.7,5HETAL=,F14.7,5HRHOV=,F14.7,
        15HRHOL=,F14.7)
104      FORMAT(6H   GAM=,F14.7,5H    L=,E14.7,5H   TH=,F14.7)
105      FORMAT(6H  TEMP=,F14.7,5H   NV=,E14.7,5H   B2=,F14.7,5H   B3=,F14.7,
        15H   XI=,F14.7)
106      FORMAT(6H    Q1=,E14.7,5H   Q2=,E14.7)
1        CONTINUE
         WRITE(3,200)
         READ(2,100) SL,RV,RW,RC,B,EPS,PHI,G,GC
         RV=RV*RW
         WRITE(3,101) SL,RV,RW,RC,B
         WRITE(3,102) EPS,PHI,G,GC
         PHI=PHI/57.29578
         PI=3.14159
         AV=PI*(RV   )**2
         AWV=PI*((RW   )**2-(RV   )**2)
         ZNV=(GAM*RHOV*ZL/ETAV)*417000000.
         XI=(G/GC)*RHOL*SL*RC*(SIN(PHI))/(2.*GAM*(COS(TH)))
         ZLAM=XI-1.
         C1=.34075
         C2=4.*(PI**2-4.)
         A1=AV/(RC*RC)
         A2=AV/AWV
         A3=B/EPS
         A4=RC/SL
         A5=A4**2
         A6=SL
         B1=ETAV*RHOL/(ETAL*RHOV)
         B2=1./B1
         B3=ZNV*   RC/(ETAV*ZL)
         B4=ZLAM
         B5=C2*COS(TH)
         B6=ETAV*ZL
         RAD=SQRT((B2*A2*A3)**2-(B3*B4*B5*A5))
         Q1=C1*A1*B6*A6*(-B2*A2*A3+RAD)
         Q2=C1*A1*B6*A6*(-B2*A2*A3-RAD)
         WRITE(3,202)
         WRITE(3,105) TEMP,ZNV,B2,B3,XI
         WRITE(3,106) Q1,Q2
         GO TO 1
         END
```

85

REFERENCES

1. Grover, G. M.; T. P. Cotter; and G. F. Erickson: Structures of Very High Thermal Conductance. Journal of Applied Physics, 35, 1990 (1964)

2. Cotter, T. P.: Theory of Heat Pipes. LA-3246-MS, Los Alamos Scientific Laboratory, Los Alamos, New Mexico, March 1965

3. Eastman, G. Y.: The Heat Pipe. Scientific American, p. 38, May 1968

4. Kemme, J. E.: Heat Pipe Capability Experiments. Proceedings of Joint Atomic Energy Commission/Sandia Laboratories Heat Pipe Conference, SC-M-66-623, Sandia Comporation, October 1966

5. Neal, L. G.: An Analytical and Experimental Study of Heat Pipes. 99900-6114-R000, TRW Systems, Redondo Beach, California, January 1967

6. Werner, R. W. and G. A. Carlson: Heat Pipe Radiator for a 50-Mwt Space Power Plant. UCRL-50294, Lawrence Radiation Laboratory, Livermore, California

7. Feldman, K. T. and G. H. Whiting: The Heat Pipe. SC-TM-66-2632, Sandia Laboratory, Albuquerque, New Mexico, March 1967

8. Deverall, J. E. and J. E. Kemme: Satellite Heat Pipe. LA-3278-MS, Los Alamos Scientific Laboratory, Los Alamos, New Mexico, April 1965

9. Anand, D. K.: On the Performance of a Heat Pipe. Journal of Spacecraft and Rockets (Engineering Notes), Vol. 3, No. 5, May 1966, pp. 763-765

10. Carnesale, A.; J. H. Cosgrove; and J. K. Ferrell: Operating Limits of the Heat Pipe. Proceedings of Joint Atomic Energy Commission/ Sandia Laboratories Heat Pipe Conference, Vol. I, SC-M-66-623, Sandia Corporation, October 1966

11. Katzoff, S.: Heat Pipes and Vapor Chambers for Thermal Control of Spacecraft. AIAA Paper No. 67-310, Presented at AIAA Thermophysics Specialist Conference, New Orleans, Louisiana, April 1967

REFERENCES - Continued

12.   Allingham, W. D. and J. A. McEntire: Determination of Boiling
      Film Coefficient for a Heated Horizontal Tube in Water-saturated
      Wick Material.   Journal of Heat Transfer, February 1961

13.   McAdams, W. H.:   Heat Transmission.   Third Edition, McGraw-
      Hill Book Company, Inc., 1954

14.   Haller, H. C.; S. Lieblein; and B. G. Lindow: Analysis and
      Evaluation of a Vapor-chamber Fin-tube Radiator for High-power
      Rankine Cycles.   NASA Technical Note TN-D-2836, Lewis Research
      Center, Cleveland, Ohio, May 1965

15.   Haller, H. C.; B. G. Lindow; and B. M. Aver: Analysis of Low-
      temperature Direct-condensing Vapor-chamber Fin and Conducting
      Fin Radiators.   NASA Technical Note TN-D-3103, Lewis Research
      Center, Cleveland, Ohio, November 1965

16.   Haller, H. C. and S. Lieblein: Analytical Comparison of Rankine
      Cycle Space Radiators Constructed of Central, Double, and Block-
      vapor Chamber Fin-tube Geometries, NASA Technical Note
      TN-D-4411, Lewis Research Center, Cleveland, Ohio, February
      1968

17.   Electronic Equipment Cooling.   Research Summary 36-I, Vol. 1,
      Jet Propulsion Laboratory, California Institute of Technology,
      February 15, 1960, pp. 64-66

18.   Gover, G. M.; J. Bondansky; and C. A. Busse: "The Use of a New
      Heat Removal System in Space Thermionic Power Supplies.
      EUR 2229.e, European Atomic Energy Community, 1965

19.   Heath, C. A. and E. Lantz: Nuclear Thermionic Space Power
      System Concept Employing Heat Pipes.   NASA Technical Note
      TN-D-4299, NASA Lewis Research Center, Cleveland, Ohio,
      March 1968

20.   Harbaugh, W. E.:   The Development of an Insulated Thermionic
      Converter-heat Pipe Assembly.   AFAPL-TR-67-45, Air Force
      Aero Propulsion Laboratory, Wright-Patterson Air Force Base,
      Ohio

21.   Campana, R. J.; L. W. Holland; and P. Hunt: Status Report on
      Heat Pipes.   GA-5676, General Dynamics, San Diego, California,
      September 1964

22. Deverall, J. E. and E. W. Salmi: Orbital Heat Pipe Experiment.
     LA-3714, Los Alamso Scientific Laboratory, Los Alamso, New Mexico,
     June 1967